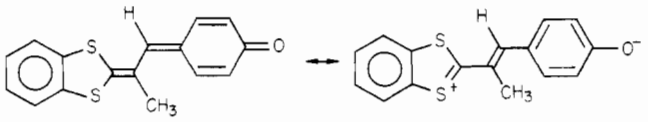

IIa IIb

Electronic $\pi \rightarrow \pi^*$ transitions of charged indicators, which are shifted bathochromically (e.g., 4-nitrophenoxide ion),[21] and all electronic spectra, which are shifted hypsochromically (i.e., all spectra wherein the magnitude of the dipole decreases in the electronic excitation) have relatively large negative *d* terms; we have encountered values ranging from −0.15 to −0.40. The same applies to ^{1}H, ^{13}C, ^{15}N, ^{19}F, ^{29}Si, and ^{119}Sn NMR shifts and coupling constants (as well as the ^{77}Se and ^{125}Te shifts reported here). As has been mentioned, values of *d* have generally been lower for infrared $\tilde{\nu}$ results, generally ranging from −0.05 to −0.15.

In sharp contrast with the trend reported here for the NMR results, −*d* values for free energies of transfer between solvents seem to decrease with decreasing solute dipolarity. We have reported[22] values near *nil* for toluene and dioxane solutes, −0.09 for the 2-butanone solute, −0.20 for the nitromethane solute, and −0.17 for the $Et_4N^+I^-$ ion pair. As concerns reaction rates, we have encountered *d* values of −0.09 to −0.17 for various types of Menschutkin reactions, but we have been unable to relate *d* to transition-state dipolarity or structure. Thus, we have encountered both larger and smaller −*d* values for reactions with less dipolar transition states.

Acknowledgment. The work by R.W.T. was done in part under a grant from the Public Health Service. The work by M.J.K. was done under Naval Surface Weapons Center Foundational Research Task No. IR-210.

Registry No. I, 14729-20-5; ^{77}Se, 14681-72-2; Me_2Se, 593-79-3; ^{125}Te, 14390-73-9; Mn_2Te, 593-80-6.

(21) Abboud, J. L. M.; Taft, R. W.; Kamlet, M. J. *Bull. Chem. Soc. Jpn.* **1982**, *55*, 603.

(22) Kamlet, M. J.; Carr, P. W.; Taft, R. W.; Abraham, M. H. *J. Chem. Soc., Faraday Trans. 1* **1982**, *78*, 1689.

Contribution from Bell Laboratories,
Murray Hill, New Jersey 07974

Electronic Structure and Bonding in the Disulfur and Diselenium Complexes $[M(X_2)(PH_3)_4]^+$ (M = Rh, Ir; X = S, Se)

A. P. GINSBERG,* J. H. OSBORNE,[1] and C. R. SPRINKLE

Received April 28, 1982

SCF-Xα-SW calculations have been carried out on the model compounds $[M(X_2)(PH_3)_4]^+$ (M = Rh, Ir; X = S, Se) in order to investigate the electronic structure and bonding in complexes of side-on-bonded disulfur and diselenium. In agreement with experiment, the calculations predict an X-X bond order of about 1 and reveal that the M-X_2 covalent interaction increases along the sequence $RhSe_2 < IrSe_2 < RhS_2 < IrS_2$. Relativistic effects partly account for the increase in interaction from Rh to Ir. The side-on-bonded S_2 and Se_2 groups are best described as molecules with excited configuration $...(p\sigma)^2(\pi)^3(\pi^*)^3$. The M-$S_2$ or M-Se_2 bond consists of in-plane π overlap of an S_2 or Se_2 $\pi_\parallel^*$ orbital with a metal $p_x + d_{xz}$ hybrid of predominantly p_x character and of σ overlap of a metal $d_{z^2} + p_z$ hybrid with S_2 or Se_2 $\pi_\parallel$ and pσ orbitals. Optical spectra of $[M(X_2)(dppe)_2]^+$ in EPA glasses at liquid-nitrogen temperature are reported for the 300-800-nm region. All bands are assigned, and acceptable agreement is found between observed and calculated transition energies. The HOMO → LUMO transition occurs as a weak band in the 530-700-nm region; it is primarily intraligand (S_2 or Se_2) in character. The lowest energy strong band is associated with the transition from the M-X_2 π-bonding orbital to the LUMO; it shifts to higher energy from M = Rh to M = Ir on account of the increase in M-X_2 interaction.

Introduction

Disulfur and diselenium can bond to metals in a variety of bridging geometries and also as terminal groups in the side-on manner[2]

Side-on-bonded S_2 and Se_2 complexes are, of course, analogues of the well-known side-on-bonded dioxygen complexes, but unlike the case of the dioxygen complexes, their chemistry has been relatively little studied, and there is no reliable information on their electronic structure. Recent work, especially the preparation of novel new disulfur complexes[3] and the discovery of the addition of low-valent-metal complexes across the S-S and Se-Se bond,[4-6] indicates that further studies on the chemistry of side-on-bonded S_2 and Se_2 are likely to yield interesting results. As a guide for future work, and for interpretation of experimental results, it would be valuable to have detailed information about the electronic structure and bonding in the

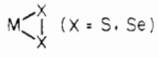

group. This paper provides such information from an SCF-Xα-SW investigation of the electronic structure of the complexes $[M(X_2)(PH_3)_4]^+$ (M = Rh, Ir; X = S, Se).

The complexes $[M(X_2)(PH_3)_4]^+$ are models for the compounds $[M(X_2)(L-L)_2]^+$ (M = Rh, Ir; X = S, Se; L-L = dppe, dmpe), and the calculations are in good agrement with

(1) 1981 summer research student at Bell Laboratories. Present address: Department of Chemistry, University of Washington, Seattle, WA.
(2) For a summary of types of metal-disulfur geometries see A. Müller and M. Jagermann, *Inorg. Chem.*, **18**, 2631 (1979).
(3) Examples: $(NH_4)_2[(S_2)_2Mo(S_2)_2Mo(S_2)_2]$ by A. Müller, W. Nolte, and B. Krebs *Angew. Chem., Int. Ed. Engl.*, **17**, 279 (1978); $(NH_4)_2[Mo_3S(S_2)_6]$ by A. Müller, S. Sarkar, R. G. Bhattacharyya, S. Pohl, and M. Dartmann, *ibid.*, **17**, 535 (1978); $[(CH_3)_4N]_2[Mo_2O_2S_2(S_2)_2]$ by W. Rittner, A. Müller, A. Neumann, W. Bather, and R. C. Sharma, *ibid.*, **18**, 530 (1979).
(4) D. Seyferth, R. S. Henderson, and M. K. Gallagher, *J. Organomet. Chem.* **193**, C75 (1980).
(5) D. A. Lesch and T. B. Rauchfuss, *J. Organomet. Chem.*, **199**, C6 (1980).
(6) A. P. Ginsberg, W. E. Lindsell, C. R. Sprinkle, K. W. West, and R. L. Cohen, *Inorg. Chem.*, **21**, 3666 (1982).

0020-1669/83/1322-0254$01.50/0

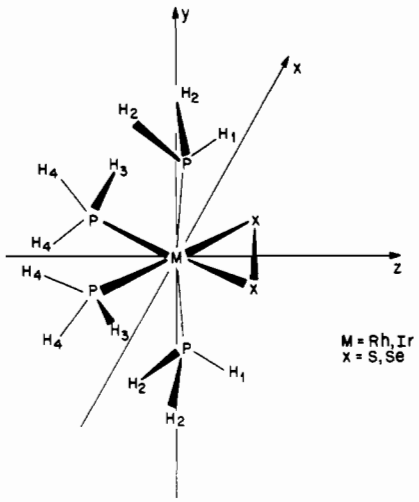

Figure 1. Coordinate axes, geometry, and atom labeling scheme for $[M(X_2)(PH_3)_4]^+$ (C_{2v}).

what is known about them.[6-8] For example, we predict the correct X–X bond order (about 1) for the X_2 group and find that the M–X_2 covalent interaction increases along the sequence $RhSe_2 < IrSe_2 < RhS_2 < IrS_2$, in agreement with experimental observations on the ease with which S and Se transfer reactions occur.[6] The increase in M–S_2 or M–Se_2 covalent interaction from Rh to Ir is shown to be partly a relativistic effect. In-plane π overlap of an S_2 or Se_2 $\pi_\parallel^*$ orbital with a metal $p_x + d_{xz}$ hybrid of predominantly p_x character and σ overlap of a metal $d_{z^2} + p_z$ hybrid with S_2 or Se_2 $\pi_\parallel$ and $p\sigma$ orbitals give rise to the M–S_2 and M–Se_2 bonds. Both the π and σ components of the bond differ from what is expected on the basis of the Dewar–Chatt model for bonding in this type of compound. The Xα calculations lead us to describe the compounds as containing S_2 or Se_2 molecules with excited configuration $...(p\sigma)^2(\pi)^3(\pi^*)^3$. This is consistent with Mason's excited-state model for the bonding of small molecules to metals[9] but contrasts with the Xα-based description of $[M(O)_2(PH_3)_4]^+$ as an O_2^{2-} complex of d^6 M(III)[10] and of $Pt(O_2)(PH_3)_2$ as an O_2^{2-} complex of d^8 Pt(II).[11a] In fact, the excited-state model is an equally valid description of the Xα results for $[M(O_2)(PH_3)_4]^+$ and $Pt(O_2)(PH_3)_2$; it provides a consistent viewpoint for understanding the electronic structure of all of these compounds. In the case of $Pt(O_2)(PH_3)_2$, Norman[11b] has already pointed out that the Xα results roughly confirm the excited-state picture.

Optical spectra of $[M(X_2)(L\text{–}L)_2]^+$ complexes in acetonitrile solution at room temperature have been reported.[6] In this paper we report spectra with improved resolution in the 300–800-nm region for $[M(X_2)(dppe)_2]^+$ (M = Rh, Ir; X = S, Se), measured in EPA glasses at liquid-nitrogen temperature. All bands are assigned, and acceptable agreement is found betwen observed and calculated transition energies. The HOMO → LUMO transition is observed as a weak band in the 530–700-nm region of all of the complexes (in the Ir complexes, both the singlet and triplet transitions are seen); it is found to be primarily intraligand (S_2 or Se_2) in character, rather than L → M charge transfer as in the dioxygen complexes. Increased strength of the Ir–X_2 interaction compared to Rh–X_2 is manifested in the optical spectra by a shift of the absorption bands of the Ir complex to energy higher than that of the corresponding bands in the rhodium complex. The first strong band in the $[M(X_2)(dppe)_2]^+$ spectra is associated with the singlet transition from the M–X_2 π-bonding orbital to the LUMO.

Table I. Bond Lengths (Å) and Angles (deg) Assumed for $[M(X_2)(PH_3)_4]^+$ (M = Rh, Ir) Complexes (C_{2v})

	X = S	X = Se
d(X–X)	2.066	2.312
d(M–X)	2.406	2.534
d(M–P_{ax})	2.367	2.377
d(M–P_{eq})	2.334	2.332
d(P–H)	1.415	1.415
∠P_{ax}–M–P_{ax}	171.6	172.7
∠P_{eq}–M–P_{eq}	98.5	97.7
∠H–P–H	93.45	93.45

Table II. Sphere Radii (bohrs) for $[M(X_2)(PH_3)_4]^+$

	M = Rh, X = S	M = Rh, X = Se	M = Ir, X = S	M = Ir, X = Se
M	2.4760	2.4961	2.5846	2.6059
X	2.4926	2.7302	2.4647	2.6982
P_{ax}	2.3636	2.3651	2.3430	2.3448
P_{eq}	2.3603	2.3597	2.3383	2.3377
H1	1.4621	1.4619	1.4616	1.4614
H2	1.4624	1.4626	1.4619	1.4621
H3	1.4630	1.4632	1.4625	1.4627
H4	1.4624	1.4624	1.4619	1.4619
OUT[a]	7.8026[b]	7.8231[c]	7.8024[d]	7.8225[e]

[a] OUT refers to the outer sphere surrounding the entire cluster. [b] $\alpha_{OUT} = 0.73335$. [c] $\alpha_{OUT} = 0.72919$. [d] $\alpha_{OUT} = 0.73333$. [e] $\alpha_{OUT} = 0.72765$.

Procedure for Calculations

SCF–Xα–SW calculations[12,13] were carried out in single precision on a Cray 1 computer with revised versions[14] of the programs written originally by K. H. Johnson and F. C. Smith. The program package includes the code by Wood and Boring, which applies relativistic mass–velocity and Darwin corrections to the calculations.[15]

Figure 1 shows the coordinate axes, conformation, and atom numbering for the C_{2v} complexes $[M(X_2)(PH_3)_4]^+$ (M = Rh, Ir; X = S, Se). Coordinates in atomic units (1 bohr = 0.529 17 Å) were derived from the geometrical parameters listed in Table I. Except for d(P–H) and ∠H–P–H, the bond distances and angles in Table I are averaged values from the X-ray structures of $[Ir(S_2)(dppe)_2]Cl$[8] and $[Ir(Se_2)(dppe)_2]Cl$.[6] The values for d(P–H) and ∠H–P–H are from the structure of the PH_3 molecule.[16,17] Although there are no X-ray structural data for disulfur or diselenium complexes of rhodium, the structure of $[Rh(O_2)(dppe)_2]^+$ has nearly the same distances and angles as $[Ir(O_2)(dppe)_2]^+$.[18,19] In view of this, we assumed the same structural parameters for $[Rh(X_2)(PH_3)_4]^+$ as for $[Ir(X_2)(PH_3)_4]^+$. Overlapping atomic sphere radii were taken as 88% of the atomic number radii[20] and are listed in Table II. These values gave satisfactory virial ratios ($-2T/V = 1.000\,023 \pm 0.000\,004$) and were not further optimized. The outer sphere surrounding the molecule was taken tangent to the H2 spheres and was centered at the valence-electron-weighted average of the atom positions. A Watson sphere,[21]

(7) A. P. Ginsberg and W. E. Lindsell, *Chem. Commun.*, 232 (1971).
(8) W. D. Bonds and J. A. Ibers, *J. Am. Chem. Soc.*, **94**, 3413 (1972).
(9) R. Mason, *Nature (London)*, **217**, 543 (1968).
(10) J. G. Norman, Jr., and P. B. Ryan, *Inorg. Chem.*, **21**, 3555 (1982).
(11) (a) J. G. Norman, Jr., *Inorg. Chem.*, **16**, 1328 (1977); (b) J. G. Norman, Jr., *J. Am. Chem. Soc.*, **96**, 3327 (1974).
(12) J. C. Slater, "The Self-consistent Field for Molecules and Solids: Quantum Theory of Molecules and Solids", Vol. 4, McGraw-Hill, New York, 1974.
(13) J. C. Slater, "The Calculation of Molecular Orbitals", Wiley, New York, 1979.
(14) Locally modified version of the revision by Mike Cook, Bruce Bursten, and George Stanley.
(15) J. H. Wood and A. M. Boring, *Phys. Rev. B: Solid State*, **18**, 2701 (1978).
(16) K. Kuchitsu, *J. Mol. Spectrosc.* **7**, 399 (1961).
(17) M. H. Sirvetz and R. E. Weston, *J. Chem. Phys.*, **21**, 898 (1953).
(18) J. A. McGinnety, N. C. Payne, and J. A. Ibers, *J. Am. Chem. Soc.*, **91**, 6301 (1969).
(19) M. J. Nolte, E. Singleton, and M. Laing, *J. Am. Chem. Soc.*, **97**, 6396 (1975).
(20) J. G. Norman, Jr., *Mol. Phys.*, **31**, 1191 (1976).
(21) R. E. Watson, *Phys. Rev.*, **111**, 1108 (1958).

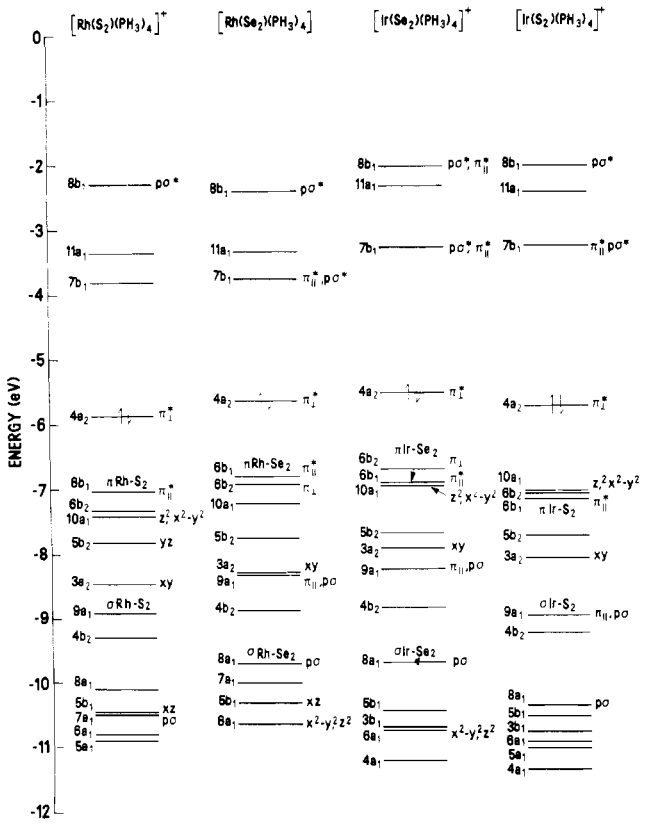

Figure 2. SCF valence energy levels for $[Rh(S_2)(PH_3)_4]^+$, $[Rh(Se_2)(PH_3)_4]^+$, $[Ir(S_2)(PH_3)_4]^+$, and $[Ir(Se_2)(PH_3)_4]^+$ above −15 eV. Purely PH_3 P–H bonding orbitals have been omitted from the diagram. The highest occupied level is marked by paired arrows. The most imporant M–X_2 bonding orbitals are designated as π M–X_2 or σ M–X_2 to indicate respectively in-plane π and σ interactions. Levels in which there is a *relative* charge[28] of 50% or more in the Rh, Ir, 2S, or 2Se atomic sphere are labeled with the spherical harmonic basis functions that contribute at least 20% of the charge in that region. Metal atom basis functions are indicated by their Cartesian representations.

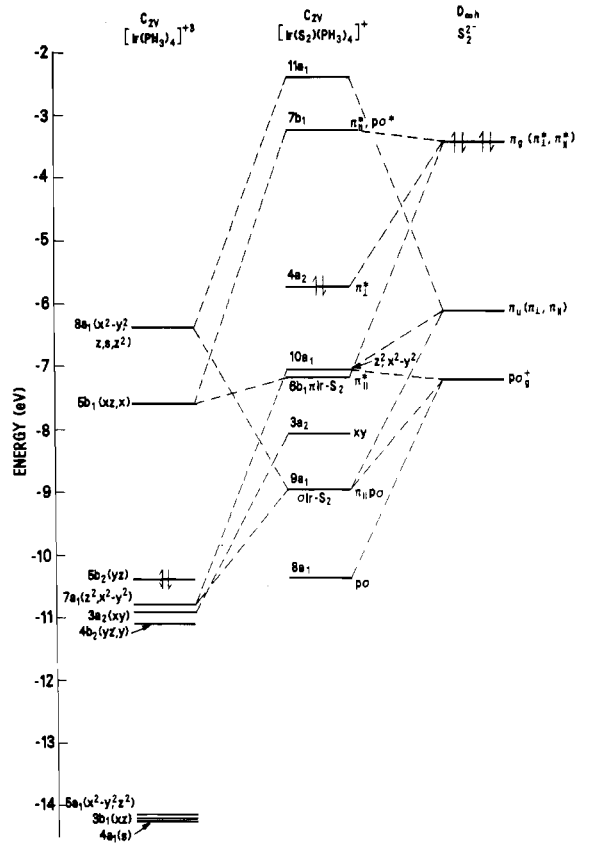

Figure 3. Simplified orbital interaction diagram for $[Ir(PH_3)_4]^{3+}$ (C_{2v}) + S_2^{2-} ($D_{\infty h}$) → $[Ir(S_2)(PH_3)_4]^+$ (C_{2v}). The most important interactions contributing to Ir–S_2 bonding are shown. All valence levels of the $[Ir(PH_3)_4]^{3+}$ fragment are shown except for PH_3 P–H bonding orbitals. With the exception of level $4a_1$, the fragment orbitals have their charge predominantly in the Ir sphere ($7a_1$ and $3a_2$ are almost pure metal orbitals); $4a_1$ has more charge on equatorial phosphorus (44%) than Ir (34%). The Ir atom basis functions contributing to the fragment orbitals are listed in order of decreasing importance next to each level. The labeling of the levels for the complex is as in Figure 2.

bearing a 1− charge and having the same radius and center as the outer sphere, was used to simulate the electrostatic interaction of the complex with its surrounding crystal lattice. α exchange-correlation parameter values were $\alpha_{Rh} = 0.702\,17$, $\alpha_{Ir} = 0.692\,96$, $\alpha_P = 0.726\,20$, $\alpha_S = 0.724\,75$, $\alpha_{Se} = 0.706\,38$, and $\alpha_H = 0.777\,25$. These values are from Schwarz's tables,[22,23] except for α_H, which is that recommended by Slater.[24] In the extramolecular and intersphere regions α was taken as an average of the atomic sphere α values weighted by the number of valence electrons in the neutral atoms (Table II).

The initial cluster potential for $[M(X_2)(PH_3)_4]^+$ was constructed by superposing SCF–Xα charge densities for Rh^+ or Ir^+, S^0 or Se^0, P^0, and H^0. Partial waves through $l = 5$ in the extramolecular region, $l = 3$ in the metal sphere, $l = 2$ in the sulfur, selenium, and phosphorus spheres, and $l = 0$ in the hydrogen spheres were used to expand the wave functions. C_{2v} symmetry was used to factor the secular matrix. The spin-restricted nonrelativistic ground-state calculations required about 12 s of Cray 1 processor time per iteration and converged in about 30 iterations to ±0.0001 Ry or better for the valence and core levels. A weighted average of the initial and final potentials for a given iteration was used as the starting potential for the next iteration; the porportion of final potential in the average varied from 10 to 25%. Relativistic effects were included in the calculations for the iridium complexes, starting with the converged nonrelatistic potentials. An additional 24 iterations (~12 s/iteration) was required to converge the relativistic calculations to ±0.0001 Ry or better for the valence levels.

The final $[M(X_2)(PH_3)_4]^+$ ground-state potentials (nonrelativistic for M = Rh; relativistic for M = Ir) were used to search for excited-state levels up to a maximum energy of −0.002 Ry. These potentials then served as the starting point for SCF calculations of the Slater transition states for 1-e transitions to the excited levels.[12,13] The transition-state calculations were carried out in spin-unrestricted form to give estimates for both singlet and triplet transition energies.

Experimental Section

$[M(X_2)(dppe)_2]Cl$ complexes[6,7] were dissolved in EPA mixed solvent (5:5:2 volume ratio of ethyl ether–isopentane–ethyl alcohol) containing a small amount of extra alcohol (19:1 EPA–ethyl alcohol). Concentrations ranged from 1×10^{-3} to 1×10^{-5} M. The solutions were frozen to clear transparent glasses at liquid-nitrogen temperature in a cylindrical quartz Dewar with an effective path length of 3.45 cm. Freezing was accomplished with a liquid-nitrogen-filled brass insert provided with an opening through which the spectrophotometer beam could pass. Spectra of the glasses were measured in the 300–800-nm region with a Cary Model 14R spectrophotometer. Extinction coefficients were corrected for solvent contraction by multiplying by 0.771, the fractional change in volume of EPA on cooling from +20 to −196 °C.[25]

Results

The calculated ground-state 1-e energies, charge distributions, and partial wave analyses for the valence molecular orbitals of $[M(X_2)(PH_3)_4]^+$ are summarized in Table III–VI. Figure 2 is a diagram of the valence energy levels of all four

(22) K. Schwarz, *Phys. Rev. B: Solid State*, **5**, 2466 (1972).
(23) K. Schwarz, *Theor. Chim. Acta*, **34**, 225 (1974).
(24) J. C. Slater, *Int. J. Quantum Chem.*, **7s**, 533 (1973).
(25) R. Passerini and I. G. Ross, *J. Sci. Instrum.*, **30**, 274 (1953).

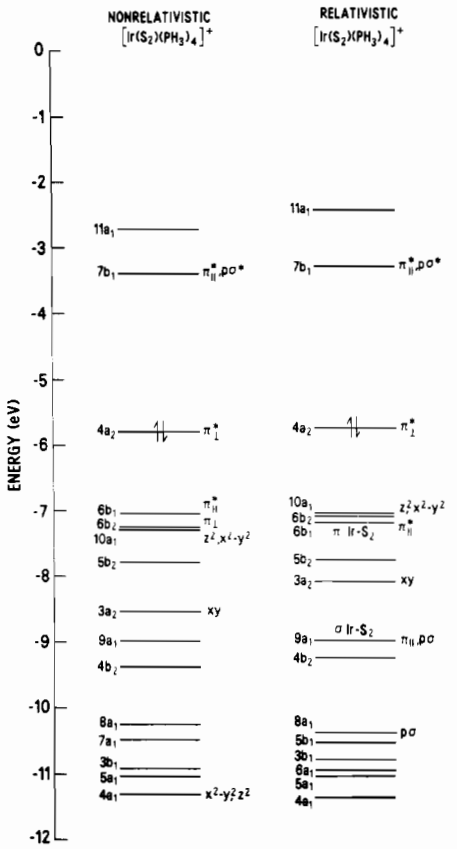

Figure 4. Comparison of the SCF valence energy levels of $[Ir(S_2)(PH_3)_4]^+$ calculated with and without relativistic corrections. Levels above −15 eV, except for pure PH_3 P–H bonding orbitals, are shown (see Figure 2 for labeling convention).

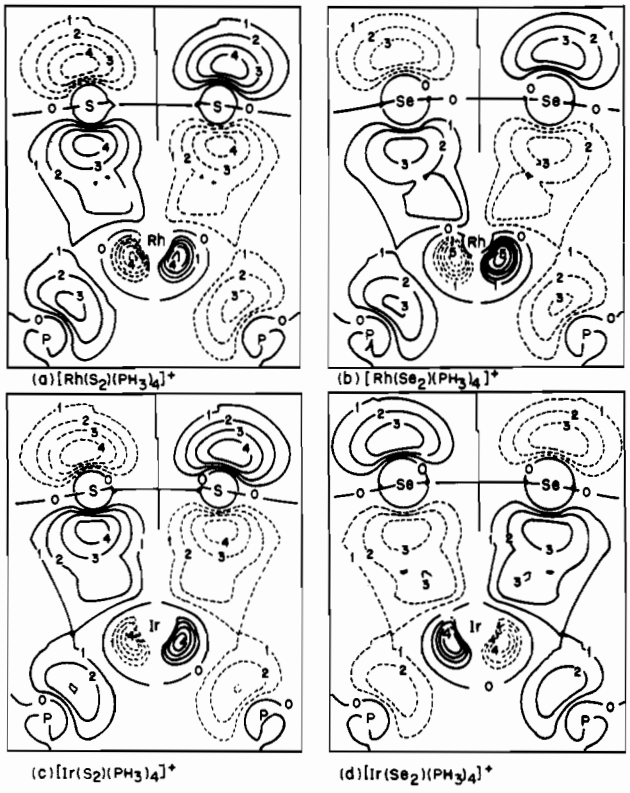

Figure 5. Wave function contour maps of the $[M(X_2)(PH_3)_4]^+$ (M = Rh, Ir; X = S, Se) $6b_1$ orbitals in the *xz* plane. Solid and broken lines denote contours of opposite sign having magnitudes indicated by the numerical labels: 0, 1, 2, 3, 4, 5 = 0, 0.05, 0.075, 0.10, 0.125, 0.16 $(e/bohr^3)^{1/2}$. Contours close to atomic centers are omitted for clarity.

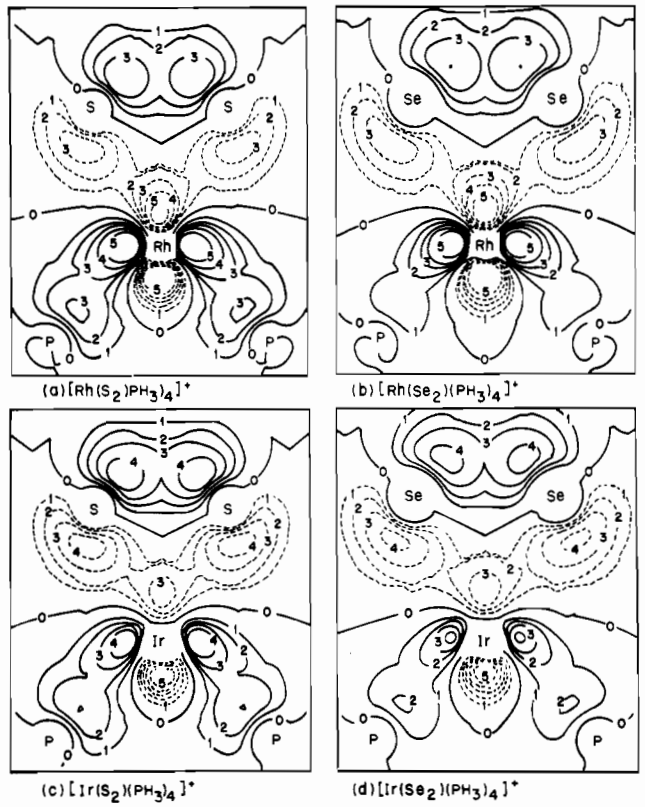

Figure 6. Wave function contour maps of the $[M(X_2)(PH_3)_4]^+$ (M = Rh, Ir; X = S, Se) $9a_1$ orbitals in the *xz* plane. Contour magnitudes and sign convention are as in Figure 5.

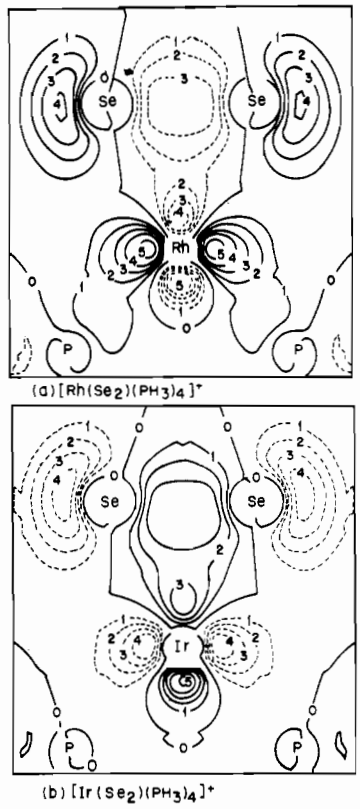

Figure 7. Wave function contour maps of the $[M(Se_2)(PH_3)_4]^+$ (M = Rh, Ir) $8a_1$ orbitals in the *xz* plane. Contour magnitudes and sign convention are as in Figure 5.

complexes, while Figure 3 correlates the valence levels of $[Ir(S_2)(PH_3)_4]^+$ with the 1-e eigenvalues of S_2^{2-} and the fragment $[Ir(PH_3)_4]^{3+}$.[26,27] The effect of the relativistic

Table III. Valence Molecular Orbitals of $[Rh(S_2)(PH_3)_4]^+$

		charge distribution, %[b]										basis functions[c,d]	
level[a]	energy, eV	Rh	2S	$2P_{ax}$	$2P_{eq}$	2H1	4H2	2H3	4H4	INT	OUT	Rh	S_2
$8b_1$	−2.285	6	51	0	2	0	0	1	0	30	10		$p\sigma^*$, $s\sigma^*$
$11a_1$	−3.351	36	8	26	8	2	2	0	1	11	5	$d_{x^2-y^2}$, d_{z^2}	
$7b_1$	−3.799	26	38	0	15	0	0	1	2	15	3	d_{xz}	$\pi_\parallel^*$, $p\sigma^*$
$4a_2$	−5.862	4	72	0	0	0	0	0	0	22	1		$\pi_\perp^*$
$6b_1$	−7.032	11	42	1	21	0	1	3	2	17	2	p_x, d_{xz}	$\pi_\parallel^*$
$6b_2$	−7.296	16	40	25	0	0	4	0	0	14	2	d_{yz}, p_y	$\pi_\perp$
$10a_1$	−7.386	49	20	0	12	0	0	0	5	12	1	d_{z^2}, $d_{x^2-y^2}$	$\pi_\parallel$, $p\sigma$
$5b_2$	−7.794	44	4	27	2	1	6	0	3	12	1	d_{yz}	
$3a_2$	−8.452	79	2	3	2	0	4	0	2	8	0	d_{xy}	
$9a_1$	−8.918	32	35	1	18	0	1	3	1	8	1	d_{z^2}, $d_{x^2-y^2}$	$\pi_\parallel$, $p\sigma$
$4b_2$	−9.270	31	29	17	0	12	0	0	0	11	1	d_{yz}	$\pi_\perp$
$8a_1$	−10.184	15	31	11	19	1	3	3	2	15	1	s	$\pi_\parallel$, $p\sigma$
$5b_1$	−10.451	52	7	3	25	0	3	1	5	3	1	d_{xz}	
$7a_1$	−10.467	12	59	7	7	2	0	6	3	3	1	$d_{x^2-y^2}$, s	$p\sigma$
$2a_2$	−10.617	0	0	22	24	0	24	0	28	0	2		
$3b_2$	−10.780	1	2	20	26	12	9	0	29	0	2		
$4b_1$	−10.794	0	0	1	46	0	1	34	16	0	2		
$6a_1$	−10.804	28	2	34	5	10	18	0	2	0	1	$d_{x^2-y^2}$, d_{z^2}	
$3b_1$	−10.865	2	0	44	3	0	48	0	1	0	2		
$5a_1$	−10.872	25	11	34	1	25	3	0	0	0	1	$d_{x^2-y^2}$, d_{z^2}	$\pi_\parallel$, $p\sigma$, $s\sigma$
$4a_1$	−11.066	6	11	1	39	1	0	27	12	1	2		$p\sigma$
$1a_2$	−11.190	4	0	24	22	0	25	0	23	1	2		
$2b_2$	−11.257	5	2	23	21	16	7	0	22	3	2		
$2b_1$	−15.960	3	87	0	0	0	0	0	0	10	0		$s\sigma^*$
$3a_1$	−17.362	2	0	41	25	7	13	4	8	0	1		
$1b_2$	−17.388	1	0	66	0	11	22	0	0	0	1		
$1b_1$	−17.443	1	0	0	66	0	0	10	21	0	1		
$2a_1$	−17.632	1	1	25	42	4	8	6	13	0	1		
$1a_1$	−20.548	3	97	0	0	0	0	0	0	0	0		$s\sigma$, $p\sigma$

[a] The highest occupied level is $4a_2$. [b] Percentage of the total population of the level located within the indicated region. Rh refers to the rhodium atomic sphere, 2S to the combined sulfur spheres. $2P_{ax}$ to the combined axial phosphorus spheres, etc. INT refers to the intersphere region and OUT to the extramolecular region. [c] When more than 10% of the population of a level is located within the Rh, 2S, or 2Se sphere, the spherical harmonic basis functions contributing more than 10% of the charge in that region are listed in order of decreasing importance. In the symbols for the S_2 and Se_2 basis functions, superscript * designates an antibonding combination, while subscripts $\parallel$ and $\perp$ indicate respectively that the orbital has its nodal plane perpendicular and parallel to the molecular plane. [d] Not shown in the table are 11% S d in level $7b_1$ and 17% S d in level $8b_1$.

Table IV. Valence Molecular Orbitals of $[Rh(Se_2)(PH_3)_4]^+$

		charge distribution, %[b]										basis functions[c,d]	
level[a]	energy, eV	Rh	2Se	$2P_{ax}$	$2P_{eq}$	2H1	4H2	2H3	4H4	INT	OUT	Rh	Se_2
$8b_1$	−2.406	8	53	0	3	0	0	1	0	25	10		$p\sigma^*$, $s\sigma^*$
$11a_1$	−3.281	36	8	26	8	2	2	0	1	11	5	$d_{x^2-y^2}$, d_{z^2}	
$7b_1$	−3.761	23	40	0	14	0	0	1	2	17	4	d_{xz}	$\pi_\parallel^*$, $p\sigma^*$
$4a_2$	−5.639	4	72	0	0	0	0	0	0	22	2		$\pi_\perp^*$
$6b_1$	−6.802	13	42	1	20	0	1	3	1	17	3	p_x, d_{xz}	$\pi_\parallel^*$
$6b_2$	−6.927	14	52	14	0	0	2	0	0	16	2	d_{yz}	$\pi_\perp$
$10a_1$	−7.225	42	26	0	12	0	0	0	4	12	2	d_{z^2}, $d_{x^2-y^2}$, p_z	$\pi_\parallel$, $p\sigma$
$5b_2$	−7.760	39	1	34	2	1	7	0	3	12	2	d_{yz}, p_y	
$3a_2$	−8.295	80	2	3	2	0	4	0	2	8	0	d_{xy}	
$9a_1$	−8.307	30	51	0	8	0	0	1	0	8	1	d_{z^2}, $d_{x^2-y^2}$	$\pi_\parallel$, $p\sigma$
$4b_2$	−8.872	40	21	18	0	10	0	0	0	11	1	d_{yz}	$\pi_\perp$
$8a_1$	−9.691	19	57	1	11	0	1	5	0	5	1	d_{z^2}, $d_{x^2-y^2}$	$p\sigma$
$7a_1$	−10.003	18	27	9	22	1	2	1	6	13	2	s, d_{z^2}	$\pi_\parallel$, $p\sigma$
$5b_1$	−10.327	53	6	2	27	0	2	2	4	3	1	d_{xz}	
$2a_2$	−10.553	0	0	20	26	0	22	0	30	0	2		
$6a_1$	−10.648	54	2	29	4	1	7	0	0	3	1	$d_{x^2-y^2}$, d_{z^2}	
$4b_1$	−10.710	0	0	0	46	0	0	34	17	0	2		
$3b_2$	−10.715	0	1	20	26	12	9	0	29	0	2		
$3b_1$	−10.826	2	0	45	2	0	48	0	1	0	2		
$5a_1$	−10.839	2	2	40	6	31	13	3	3	0	2		
$4a_1$	−10.957	3	1	7	39	5	2	28	13	0	2		
$1a_2$	−11.132	3	0	26	21	0	27	0	21	1	2		
$2b_2$	−11.201	4	1	25	20	18	8	0	20	2	2		
$2b_1$	−15.837	2	89	0	0	0	0	0	0	8	1		$s\sigma^*$
$3a_1$	−17.312	2	0	36	30	6	11	5	10	0	1		
$1b_1$	−17.362	1	0	0	66	0	0	10	21	0	1		
$1b_2$	−17.367	1	0	66	0	11	21	0	0	0	1		
$2a_1$	−17.570	1	2	29	36	4	9	5	12	0	1		
$1a_1$	−19.210	3	96	1	0	0	0	0	0	0	0		$s\sigma$

[a] The highest occupied level is $4a_2$. [b] See Table III, footnote *b*. [c] See Table III, footnote *c*. [d] Not shown in the table is 13% Se d in level $8b_1$.

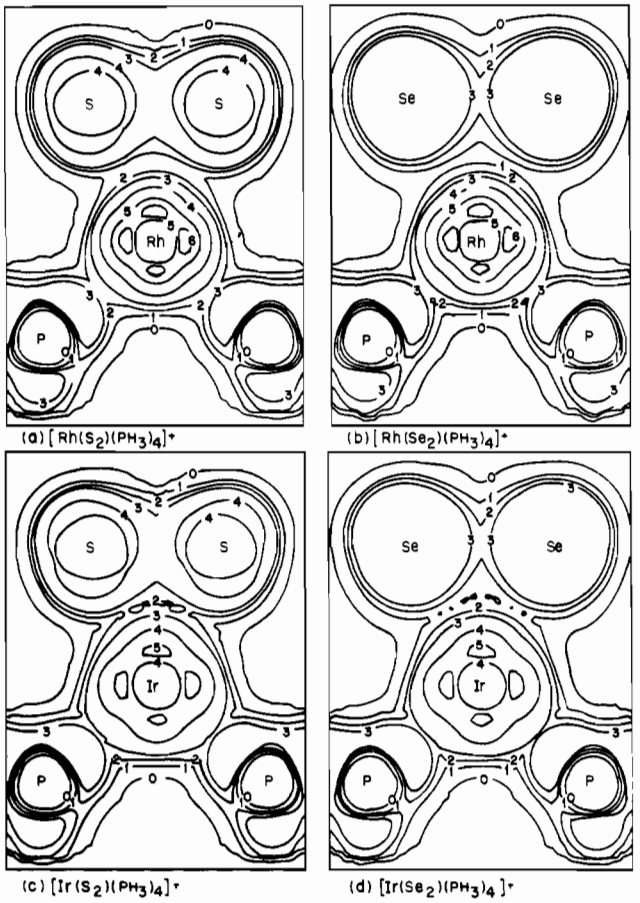

Figure 8. Total valence charge density contour maps for $[M(X_2)(PH_3)_4]^+$ (M = Rh, Ir; X = S, Se). Contour values: 0, 1, 2, 3, 4, 5, 6 = 0.014, 0.028, 0.035, 0.042, 0.070, 0.140, 0.210 (e/bohr^3).

corrections is exhibited in Figure 4, which compares the relativistic and nonrelativistic energy levels of $[Ir(S_2)(PH_3)_4]^+$. Wave function contour maps of selected orbitals are shown in Figures 5–7. Total valence charge density contour maps are exhibited in Figures 8 and 9.

Table VII gives the calculated total charge distributions as well as estimated net atomic charges. The absolute values of the net atomic charges are questionable since they depend on a rather crude method of assigning the intersphere and extramolecular charge to the atomic spheres (footnote *a*, Table VII). However, in view of the near constancy of the intersphere and extramolecular charge for the four complexes, we believe the differences between the net charges in the different complexes to be reliable. For the same reason we expect differences among the metal atom, S_2, and Se_2 orbital occupancies given in Table VIII to be significant, although the occupancy values themselves may not be very accurate. Values >2.00 in Table VIII result from improper assignment of the intersphere and extramolecular charge. The observed electronic absorptions and the calculated transition-state energies are presented in Tables X–XIII.

Discussion

The occupied valence molecular orbitals of the four $[M(X_2)(PH_3)_4]^+$ complexes have energies in the range −20.6 to −5.5 eV. In each case the HOMO (highest occupied molecular orbital) is level $4a_2$, a nearly pure S_2 or Se_2 $\pi_\perp^*$ orbital. In general, the ligand and metal orbitals are extensively mixed in the MO's; the only exceptions are the $\pi_\perp^*$ orbital and the metal d_{xy} orbital (level $3a_2$), which are essentially noninteracting.

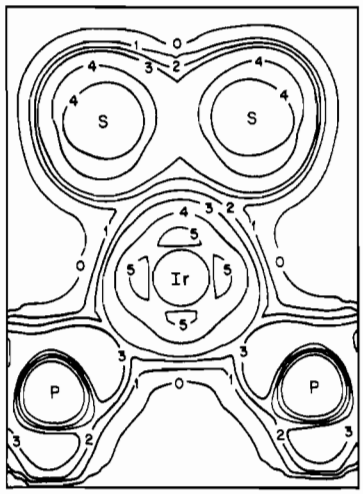

Figure 9. Total valence charge density contour map for nonrelativistic $[Ir(S_2)(PH_3)_4]^+$. Contour values are the same as those in Figure 8.

Examination of Tables III–VI and Figure 2 suggests that the occupied valence-level MO's may be divided into the following five more or less well-defined groups, given in order of decreasing energy: First, there are three orbitals, $4a_2$, $6b_1$, and $6b_2$, in which the most important components are respectively S_2 or Se_2 $\pi_\perp^*$, $\pi_\parallel^*$, and $\pi_\perp$. Level $6b_1$ is the in-plane π M–X_2 bonding orbital. Next are three orbitals, $10a_1$, $5b_2$, and $3a_2$ (in $[Ir(S_2)(PH_3)_4]^+$ level $10a_1$ occurs between $4a_2$ and $6b_2$ of the first group), which have large metal atom components. Third, in the Rh complexes is a group of five orbitals, $9a_1$, $4b_2$, $8a_1$, $5b_1$, and $7a_1$, which contribute to σ M–X_2 or M–P bonding. A similar group is found in the Ir complexes, but here level $7a_1$ is a pure P–H bonding orbital and falls into the following group while level $2a_2$, also a P–H bonding orbital, occurs between $8a_1$ and $5b_1$. The fourth group consists of nine orbitals occurring between ca. −10.5 and −11.4 eV; these are predominantly P–H bonding in character, but among them also are found M–P bonding orbitals. Following the fourth group of levels there is a gap of ca. 4.6 eV before the last group of valence levels begins. The highest level in this group is $2b_1$, the S_2 or Se_2 $s\sigma^*$ orbital; the lowest level in the group is $1a_1$, the S_2 or Se_2 $s\sigma$ orbital. Between $2b_1$ and $1a_1$ are found four P–H bonding orbitals.

In addition to the occupied levels, Table III–VI and Figure 2 show three empty levels, $7b_1$, $11a_1$, and $8b_1$, for each complex. The LUMO (lowest unoccupied molecular orbital), $7b_1$, has its largest component on S_2 or Se_2 and, except for $[Ir(Se_2)(PH_3)_4]^+$, is predominantly $\pi_\parallel^*$ with a substantial (18–39%) $p\sigma^*$ contribution. In $[Ir(Se_2)(PH_3)_4]^+$ the Se_2 component of the LUMO is predominantly $p\sigma^*$ with about 38% $\pi_\parallel^*$. Contour maps show the LUMO to be mainly M–X and X–X antibonding in character. Next above the LUMO, orbital $11a_1$ has large components on the metal and on the axial phosphorus atoms. The metal atom component is a predominantly $d_{x^2-y^2}$ hybrid with d_{z^2} (about 33% d_{z^2} and 65% $d_{x^2-y^2}$), and the orbital is mainly M–P_{ax} antibonding in character. The highest energy unoccupied orbital shown in the tables is level $8b_1$, which has its major component on S_2 or Se_2 and is a predominantly $p\sigma^*$ hybrid with $s\sigma^*$ and, in the Ir complexes, $\pi_\parallel^*$.

M–S_2 and M–Se_2 Bonding. Examination of contour maps shows that the greatest single contribution to the M–S_2 or

(26) The $[Ir(PH_3)_4]^{3+}$ fragment was assumed to have the same geometry and bond distances as in $[Ir(S_2)(PH_3)_4]^+$. Overlapping atomic sphere radii were determined, and the calculation, including relativistic corrections, was carried out as described in this paper.

(27) S_2^{2-} was assumed to have the same S–S distance as in $[Ir(S_2)(dppe)_2]^+$, which is in fact practically the same as the distance in SrS_2 (2.07 Å vs. 2.08 Å). Overlapping-sphere radii were used.

(28) The relative atomic sphere charges differ from the values in Tables III–VI in being normalized so that the sum of the atomic sphere charges is 100%.

Table V. Valence Molecular Orbitals (Relativistic) of $[Ir(S_2)(PH_3)_4]^+$

		charge distribution, %[b]										basis functions[c,d]	
level[a]	energy, eV	Ir	2S	$2P_{ax}$	$2P_{eq}$	2H1	4H2	2H3	4H4	INT	OUT	Ir	S_2
$8b_1$	−2.030	14	40	0	5	0	0	1	0	29	11	d_{xz}	$p\sigma^*$, $s\sigma^*$, $\pi_\parallel^*$
$11a_1$	−2.445	36	9	22	8	2	2	0	1	13	7	$d_{x^2-y^2}$, d_{z^2}	
$7b_1$	−3.270	20	44	0	10	0	0	1	1	20	4	d_{xz}	$\pi_\parallel^*$, $p\sigma$
$4a_2$	−5.760	6	70	0	0	0	0	0	0	22	1		$\pi_\perp^*$
$10a_1$	−7.065	57	14	0	10	0	0	1	4	12	1	d_{z^2}, $d_{x^2-y^2}$	$\pi_\parallel$, $p\sigma$
$6b_2$	−7.082	39	38	5	1	0	0	0	1	15	1	d_{yz}	$\pi_\perp$
$6b_1$	−7.185	13	45	1	18	0	1	3	1	17	2	p_x, d_{xz}	$\pi_\parallel^*$
$5b_2$	−7.755	27	4	42	2	0	10	0	3	11	2	d_{yz}, p_y	
$3a_2$	−8.087	73	4	4	2	0	5	0	2	9	0	d_{xy}	
$9a_1$	−8.981	21	48	1	16	1	0	2	2	8	1	d_{z^2}, $d_{x^2-y^2}$, p_z	$\pi_\parallel$, $p\sigma$
$4b_2$	−9.265	23	29	21	0	14	0	0	0	11	1	d_{yz}, p_y	$\pi_\perp$
$8a_1$	−10.375	8	58	2	13	2	0	11	1	3	1		$p\sigma$
$2a_2$	−10.467	0	0	21	24	0	24	0	29	0	2		
$5b_1$	−10.554	33	6	16	20	0	18	0	6	0	1	d_{xz}	
$4b_1$	−10.657	2	1	0	45	0	0	36	15	0	2		
$3b_2$	−10.658	1	3	17	28	10	9	0	31	0	2		
$7a_1$	−10.740	3	2	43	1	29	19	0	0	0	2		
$8b_1$	−10.774	16	1	31	12	0	34	1	3	0	2	d_{xz}	
$6a_1$	−10.952	14	7	3	35	2	0	17	17	3	1	$d_{x^2-y^2}$	
$5a_1$	−11.036	41	20	15	10	2	2	6	0	3	1	d_{z^2}, $d_{x^2-y^2}$	$p\sigma$, $\pi_\parallel$, $s\sigma$
$1a_2$	−11.076	4	0	24	21	0	25	0	22	3	2		
$2b_2$	−11.175	6	3	24	18	16	8	0	18	5	2		
$4a_1$	−11.372	27	16	20	13	3	3	2	2	11	1	s	$\pi_\parallel$
$2b_1$	−15.997	3	86	0	0	0	0	0	0	10	0		$s\sigma^*$
$3a_1$	−17.285	2	0	38	27	6	12	4	9	0	1		
$1b_2$	−17.292	1	0	66	0	11	21	0	0	0	1		
$1b_1$	−17.355	2	0	0	66	0	0	10	21	0	1		
$2a_1$	−17.614	3	1	27	38	4	8	6	12	0	1		
$1a_1$	−20.603	5	95	0	0	0	0	0	0	0	0		$s\sigma$, $p\sigma$

[a] The highest occupied level is $4a_2$. [b] See Table III, footnote *b*. [c] See Table III, footnote *c*. [d] Not shown in the table are 16% S d in level $7b_1$ and 14% S d in level $8b_1$.

Table VI. Valence Molecular Orbitals (Relativistic) of $[Ir(Se_2)(PH_3)_4]^+$

		charge distribution, %[b]										basis functions[c,d]	
level[a]	energy, eV	Ir	2Se	$2P_{ax}$	$2P_{eq}$	2H1	4H2	2H3	4H4	INT	OUT	Ir	Se_2
$8b_1$	−2.041	17	41	0	6	0	0	1	0	22	11	d_{xz}	$p\sigma^*$, $\pi_\parallel^*$, $s\sigma^*$
$11a_1$	−2.357	36	9	22	8	2	2	0	1	13	7	$d_{x^2-y^2}$, d_{z^2}	
$7b_1$	−3.301	16	47	0	9	0	0	0	1	22	5	d_{xz}	$p\sigma^*$, $\pi_\parallel^*$
$4a_2$	−5.521	5	69	0	0	0	0	0	0	23	2		$\pi_\perp^*$
$6b_2$	−6.724	27	48	6	0	0	1	0	0	17	2	d_{yz}	$\pi_\perp$
$6b_1$	−6.913	15	45	1	16	0	1	3	1	16	3	p_x, d_{xz}	$\pi_\parallel^*$
$10a_1$	−6.955	54	17	0	9	0	0	1	4	12	2	d_{z^2}, $d_{x^2-y^2}$	$\pi_\parallel$, $p\sigma$
$5b_2$	−7.681	37	3	33	2	0	9	0	3	10	2	d_{yz}, p_y	
$3a_2$	−7.922	74	4	4	2	0	5	0	2	9	0	d_{xy}	
$9a_1$	−8.251	17	59	0	9	0	0	1	1	10	1	d_{z^2}, p_z, $d_{x^2-y^2}$	$\pi_\parallel$, $p\sigma$
$4b_2$	−8.846	27	21	27	0	11	0	0	0	12	1	d_{yz}, p_y	$\pi_\perp$
$8a_1$	−9.670	17	63	1	7	1	0	5	0	4	1	d_{z^2}, $d_{x^2-y^2}$	$p\sigma$
$2a_2$	−10.379	0	0	20	25	0	23	0	30	0	2		
$5b_1$	−10.444	39	6	12	24	0	13	1	5	0	1	d_{xz}	
$4b_1$	−10.557	1	0	0	45	0	0	35	16	0	2		
$3b_2$	−10.557	0	1	19	26	11	10	0	30	0	2		
$7a_1$	−10.682	2	3	43	2	30	18	1	1	0	2		
$3b_1$	−10.696	11	1	35	10	0	39	0	3	0	2	d_{xz}	
$6a_1$	−10.751	49	10	12	19	1	2	2	3	2	1	$d_{x^2-y^2}$, d_{z^2}	
$5a_1$	−10.826	5	2	2	42	1	1	27	16	2	2		
$1a_2$	−10.994	4	0	25	20	0	26	0	21	3	2		
$2b_2$	−11.079	5	2	25	19	17	8	0	20	4	2		
$4a_1$	−11.216	30	7	27	11	5	4	2	2	10	1	s, $d_{x^2-y^2}$	
$2b_1$	−15.817	3	88	0	0	0	0	0	0	8	1		$s\sigma^*$
$3a_1$	−17.202	2	0	37	28	6	12	4	9	0	1		
$1b_2$	−17.227	1	0	66	0	11	21	0	0	0	1		
$1b_1$	−17.259	2	0	0	66	0	0	10	21	0	1		
$2a_1$	−17.519	3	3	27	37	4	8	5	11	0	1		
$1a_1$	−19.253	4	93	1	1	0	0	0	0	0	0		$s\sigma$

[a] The highest occupied level is $4a_2$. [b] See Table III, footnote *b*. [c] See Table III, footnote *c*. [d] Not shown in the table are 14% Se d in level $7b_1$ and 11% Se d in level $8b_1$.

M–Se_2 interatomic charge density comes from the in-plane π interaction in orbital $6b_1$. In all four cases this orbital has its charge mainly in the S_2 or Se_2 spheres and the interaction is due to overlap of the S_2 or Se_2 $\pi_\parallel^*$ orbital with a Rh or Ir p_x–d_{xz} hybrid orbital that has more p_x than d_{xz} character. Contour maps of level $6b_1$ for the four complexes are shown

Table VII. Total Sphere Charges and Approximate Net Atomic Charges[a]

	$[Rh(S_2)(PH_3)_4]^+$	$[Rh(Se_2)(PH_3)_4]^+$	$[Ir(S_2)(PH_3)_4]^+$	$[Ir(Se_2)(PH_3)_4]^+$	$[Ir(PH_3)_4]^{3+}$ (C_{2v})
			Total Sphere Charge, e		
Rh or Ir	44.52	44.57	76.61	76.67	76.66
S or Se	15.55	33.50	15.51	33.45	
P_{ax}	14.27	14.26	14.23	14.23	14.26
P_{eq}	14.26	14.25	14.21	14.21	14.18
H1	1.00	1.00	1.00	1.00	1.00
H2	0.99	0.99	1.00	1.00	1.01
H3	0.99	0.99	0.99	0.99	0.99
H4	0.99	0.99	1.00	1.00	1.00
INT	2.79	2.81	2.85	2.86	0.46
OUT	0.62	0.71	0.63	0.72	0.019
			Net Charge		
Rh or Ir	0.36−	0.46−	0.54−	0.61−	0.02+
S or Se	0.24−	0.24−	0.18−	0.18−	
P_{ax}	0.53+	0.54+	0.56+	0.56+	0.70+
P_{eq}	0.54+	0.56+	0.61+	0.63+	0.81+
H1	0.04−	0.03−	0.05−	0.05−	0.01+
H2	0.02−	0.02−	0.03−	0.03−	0.01−
H3	0.02−	0.02−	0.03−	0.03−	0.01+
H4	0.02−	0.02−	0.04−	0.03−	0.00

[a] Net atomic charge = atomic no. $- \Sigma_{\text{all levels}}$(relative atomic sphere charge), where the relative atomic sphere charge is the relative percentage of the orbital charge in the atomic sphere: $\Sigma_{\text{atomic spheres}}$ relative atomic sphere charges = 100%.

in Figure 5, where the following relations between the π M–X_2 overlaps can be discerned: π Rh–Se_2 < π Ir–Se_2; π Rh–S_2 < π Ir–S_2; π Rh–Se_2 < π Rh–S_2; π Ir–Se_2 ≈ π Ir–S_2. π Rh–Se_2 has the smallest in-plane π M–X_2 overlap. The increase in π M–X_2 overlap in going from Rh to Ir is accompanied by an increase in p_x and a decrease in d_{xz} character of the metal hybrid orbital that overlaps the X_2 $\pi_\parallel$* orbital.[29] We will see in the discussion of relativistic effects that the improved π M–X_2 overlap in the iridium complexes is partly a result of the relativistic expansion of the d_{xz} orbital.

σ overlap also makes an important contribution to M–X_2 bonding. The main σ interaction occurs in orbital $9a_1$ and, for the Se_2 complexes, in orbital $8a_1$. In orbital $9a_1$ the interaction takes place between an S_2 or Se_2 $\pi_\parallel$–pσ hybrid (about 65% $\pi_\parallel$ and 35% pσ) and a d_{z^2}–$d_{x^2-y^2}$–p_z metal hybrid orbital, of which d_{z^2} is the largest component.[30] In orbital $8a_1$ the interaction takes place between an essentially pure Se_2 pσ orbital and a Rh or Ir d_{z^2}–$d_{x^2-y^2}$ hybrid orbital of which d_{z^2} is the largest component.[31] Contour maps of the $9a_1$ and $8a_1$ orbitals are shown in Figures 6 and 7. Figure 6 reveals that the M–X_2 overlap in level $9a_1$ increases along the series Rh–Se_2 ≲ Rh–S_2 < Ir–Se_2 < Ir–S_2. The M–Se_2 interaction in level $8a_1$ is seen from Figure 7 to follow the order Rh–Se_2 < Ir–Se_2. Enhanced σ M–X_2 overlap for Ir as compared to Rh is a relativistic effect (vide infra).

Another contribution to σ M–X_2 bonding comes from overlap of a Rh 5s or Ir 6s orbital with an X_2 $\pi_\parallel$–σ hybrid of mainly $\pi_\parallel$ character. In $[Rh(S_2)(PH_3)_4]^+$ this interaction occurs in level $8a_1$ while the $[Ir(S_2)(PH_3)_4]^+$ it is in level $4a_1$ and in $[Rh(Se_2)(PH_3)_4]^+$ in level $7a_1$; it is not a significant interaction in $[Ir(Se_2)(PH_3)_4]^+$. Examination of contour maps shows that in the Rh complexes the Rh 5s–X_2 $\pi_\parallel$ overlap is of about the same order as the σ overlap in level $9a_1$ but the Ir 6s–S_2 $\pi_\parallel$ interaction, although similar to the Rh 5s–X_2 $\pi_\parallel$ interaction, is less than the interaction in level $9a_1$ of $[Ir(S_2)(PH_3)_4]^+$.

All four complexes have a weak out-of-plane π-bonding interaction in level $4b_2$, but this is largely canceled by the antibonding interaction in level $6b_2$. Out-of-plane π bonding therefore does not make a significant contribution to the M–X_2 bond.

Figure 3 provides a simplified picture of the formation of the Ir–S_2 bond by interaction of an S_2^{2-} ion with the C_{2v} fragment $[Ir(PH_3)_4]^{3+}$. Interaction of the electron pair in S_2^{2-} $\pi_\parallel$* with the vacant $5b_1$ fragment orbital leads to formation of the π Ir–S_2 bonding orbital $6b_1$ and the antibonding LUMO $7b_1$. Participation of the empty S_2^{2-} pσ_u* orbital in this interaction imparts pσ* character to the LUMO. Interaction of the S_2^{2-} $\pi_\parallel$ electron pair with the empty fragment orbital $8a_1$ forms the σ Ir–S_2 bonding orbital $9a_1$ and the antibonding orbital $11a_1$. In addition, there is extensive interaction of the S_2^{2-} pσ_g* electron pair with the $8a_1$ fragment orbital leading to the pσ contribution in level $9a_1$. The M–P_{eq} bonding character of level $9a_1$ results from the participation of fragment orbital $7a_1$. These interactions are accompanied by a substantial transfer of charge from S_2^{2-} to Ir, P, and H. If we look only at the interactions described above, we find, using normalized sphere charges, that 1.85 e are transferred out of the S spheres, leaving a net charge of 0.15− on the bound S_2 group. This may be compared with the approximate net *atomic* charge of 0.18− given in Table VII for S in $[Ir(S_2)(PH_3)_4]^+$.

An assessment of the relative strength of the covalent M–X_2 interaction in the four complexes may be obtained by examining the total valence charge density maps in Figure 8. These maps indicate that the interaction follows the order

$$\text{Rh–Se}_2 < \text{Ir–Se}_2 < \text{Rh–S}_2 < \text{Ir–S}_2$$

Another measure of the strength of the M–X_2 covalent interaction is the splitting between levels $7b_1$ and $6b_1$. This follows the order

$$\text{Rh–Se}_2 < \text{Rh–S}_2 < \text{Ir–Se}_2 < \text{Ir–S}_2$$

The most important metal orbitals for bonding S_2 and Se_2 are $(n+1)p_x$, nd_{z^2}, and $(n+1)p_z$ (n = 4 for Rh and 5 for Ir); hybridization of nd_{xz} with $(n+1)p_x$ is important for good in-plane π overlap.

It it instructive to compare the description of M–S_2 and M–Se_2 bonding presented in this section with a description in terms of the Dewar–Chatt model.[32] A Dewar–Chatt description calls for X_2 p$\pi_\parallel$ → M d_σ σ bonding together with M d_π → X_2 p$\pi_\parallel$* π back-bonding. The Dewar–Chatt σ bond corresponds to the interaction in level $9a_1$ and differs from the Xα result in neglecting the contribution of the X_2 pσ electrons. The Dewar–Chatt π back-bond corresponds to the interaction in level $6b_1$. Here the Xα result is very different from the Dewar–Chatt description in two respects: (1) The orbital has more charge on S_2 or Se_2 than on the metal atom, so that the interaction should not be referred to as "back-bonding". (2) The metal atom component of orbital $6b_1$ has more p than d character.

(29) Composition of orbital $6b_1$ in the metal sphere: 54% $5p_x$, 39% $4d_{xz}$, 6% 4f for $[Rh(S_2)(PH_3)_4]^+$; 60% $6p_x$, 32% $5d_{xz}$, 8% 5f for $[Ir(S_2)(PH_3)_4]^+$; 48% $5p_x$, 48% $4d_{xz}$, 5% 4f for $[Rh(Se_2)(PH_3)_4]^+$; 54% $6p_x$, 40% $5d_{xz}$, 6% 5f for $[Ir(Se_2)(PH_3)_4]^+$. *Without* relativistic corrections the composition of orbital $6b_1$ for $[Ir(S_2)(PH_3)_4]^+$ is as follows: 62% $6p_x$, 29% $5d_{xz}$, 9% 5f.

(30) Composition of orbital $9a_1$ in the metal sphere: 58% $4d_{z^2}$, 29% $4d_{x^2-y^2}$, 9% $5p_z$, 3% 5s for $[Rh(S_2)(PH_3)_4]^+$; 49% $5d_{z^2}$, 23% $5d_{x^2-y^2}$, 23% $6p_z$, 3% 5f, 2% 6s for $[Ir(S_2)(PH_3)_4]^+$; 73% $4d_{z^2}$, 20% $4d_{x^2-y^2}$, 6% $5p_z$, 1% 4f for $[Rh(Se_2)(PH_3)_4]^+$; 62% $5d_{z^2}$, 12% $5d_{x^2-y^2}$, 22% $6p_z$, 3% 5f for $[Ir(Se_2)(PH_3)_4]^+$. *Without* relativistic corrections the composition of orbital $9a_1$ for $[Ir(S_2)(PH_3)_4]^+$ is as follows: 57% $5d_{z^2}$, 26% $5d_{x^2-y^2}$, 11% $6p_z$, 3% 6s, 2% 5f.

(31) Composition of orbital $8a_1$ in the metal sphere: 48% $4d_{z^2}$, 39% $4d_{x^2-y^2}$, 7% 5s, 5% $5p_z$ for $[Rh(Se_2)(PH_3)_4]^+$; 58% $5d_{z^2}$, 32% $5d_{x^2-y^2}$, 9% $6p_z$ for $[Ir(Se_2)(PH_3)_4]^+$.

(32) M. J. S. Dewar, *Bull. Soc. Chim. Fr.*, **18**, C79 (1951); J. Chatt and L. A. Duncanson, *J. Chem. Soc.*, 2939 (1953).

Table VIII. Approximate Assignment of Valence Electrons to Metal Atom, S_2, and Se_2 Orbitals[a]

orbital[b,c]	$[Rh(S_2)(PH_3)_4]^+$	$[Rh(Se_2)(PH_3)_4]^+$	$[Ir(S_2)(PH_3)_4]^+$	$[Ir(Se_2)(PH_3)_4]^+$	C_{2v}-$[Ir(PH_3)_4]^{3+}$	S_2^{2-}
nd	8.27	8.37	7.96	8.00	7.62	
$(n+1)p_x$	0.18	0.19	0.25	0.26	0.10	
$(n+1)p_y$	0.20 } $p^{0.57}$	0.21 } $p^{0.59}$	0.27 } $p^{0.77}$	0.28 } $p^{0.80}$	0.37 } $p^{0.55}$	
$(n+1)p_z$	0.19	0.19	0.25	0.26	0.08	
$(n+1)$s	0.43	0.43	0.684	0.688	0.70	
$\pi_\parallel{}^*$	1.11	1.08	1.17	1.14		1.94
$\pi_\perp{}^*$	1.89 } net $\pi = 0.26$	1.90 } net $\pi = 0.30$	1.87 } net $\pi = 0.11$	1.89 } net $\pi = 0.15$		1.94 } net $\pi = 0.02$
$\pi_\parallel$	1.53	1.52	1.44	1.44		1.95
$\pi_\perp$	1.73	1.76	1.71	1.74		1.95
$p\sigma^*$	0.13 } net $p\sigma = 1.92$	0.10 } net $p\sigma = 1.94$	0.13 } net $p\sigma = 1.86$	0.10 } net $p\sigma = 1.88$		0.14 } net $p\sigma = 1.92$
$p\sigma$	2.05	2.04	1.99	1.98		2.06
$s\sigma^*$	1.84 } net $s\sigma = -0.08$	1.88 } net $s\sigma = -0.02$	1.83 } net $s\sigma = -0.06$	1.88 } net $s\sigma = -0.03$		1.84 } net $s\sigma = -0.07$
$s\sigma$	1.76	1.86	1.77	1.85		1.77

[a] These approximate orbital occupancy values are the contribution to the total valence charge of the spherical harmonic basis functions. They are determined by summing over all valence levels the charge contributed to each MO by the basis function. The charge contributed by a basis function to an MO was taken as the product of the *normalized* atomic sphere charge (cf. Table VII, footnote *a*) with the fraction of the actual atomic sphere charge due to the basis function. [b] nd, $(n+1)$p, and $(n+1)$s orbitals are on Rh or Ir, with $n = 4$ for Rh and 5 for Ir. π and σ orbitals are S_2 or Se_2 MO's; see footnote *c*, Table III, for explanation of notation. [c] Net π- and σ-electron counts given for the S_2 and Se_2 orbitals are the differences between the occupancies of the bonding and antibonding orbitals.

Table IX. Summary of Orbitals in Which M–P Bonding Interactions Occur[a]

complex	equatorial M–P bonding	axial M–P bonding
$[Rh(S_2)(PH_3)_4]^+$	$5b_1$, $9a_1$, $10a_1$ (24% P 3d), $8a_1$	$5b_2$, $6b_2$, $6a_1$, $5a_1$, $4b_2$
$[Rh(Se_2)(PH_3)_4]^+$	$5b_1$, $7a_1$, $10a_1$ (22% P 3d), $8a_1$, $9a_1$	$6a_1$, $5b_2$, $4b_2$, $6b_2$
$[Ir(S_2)(PH_3)_4]^+$	$5b_1$, $9a_1$, $3b_1$, $10a_1$ (45% P 3d), $6a_1$, $4a_1$	$5b_2$, $5a_1$, $4a_1$, $4b_2$
$[Ir(Se_2)(PH_3)_4]^+$	$5b_1$, $6a_1$, $10a_1$ (45% P 3d), $9a_1$, $3b_1$	$4a_1$, $5b_2$, $4b_2$, $6a_1$
$[Ir(PH_3)_4]^{3+}(C_{2v})$	$3b_1$, $4a_1$	$5a_1$, $4b_2$, $5b_2$

[a] Orbitals are listed in approximate order of decreasing M–P interaction as judged from wave function contour maps.

Valence Electron Distribution on Rh, Ir, S_2, and Se_2. The approximate net atomic charges and orbital occupancies in Tables VII and VIII lead to some interesting conclusions. (It should be noted that most of the arguments in this section are based on *differences* of net atomic charges or orbital occupancies, which we believe to be more reliable than the absolute numbers in Tables VII and VIII.) First of all, comparison of the net π, net $p\sigma$, and net $s\sigma$ electron counts for the two S_2 complexes and for S_2^{2-}, taking the S–S bond order of S_2^{2-} to be 1, indicates that the S–S bond order in $[Rh(S_2)(PH_3)_4]^+$ is somewhat greater than 1 and that the S–S bond order in the Ir complex is less than in the Rh complex but still about 1. A similar conclusion holds for $[Rh(Se_2)(PH_3)_4]^+$ and $[Ir(Se_2)(PH_3)_4]^+$. The observed S–S and Se–Se distances in $[Ir(X_2)(dppe)_2]^+$[6,8] are in accord with these conclusions. Although the complexed S_2 and Se_2 groups have a bond order near 1, it is clear from Table VIII that they are quite different from disulfide or diselenide. It is more consistent with the Xα results to think of them as S_2 or Se_2 molecules in an excited state with the electron configuration $...(p\sigma)^2(\pi)^3(\pi^*)^3$. This description takes account of both the bond order and charge distribution of the bound S_2 or Se_2 group; it agrees with Mason's[9] excited-state model for the binding of small molecules in complexes. The earliest discussions of side-on-bonded disulfur complexes[7,8,33] suggested that they be viewed as containing molecular S_2 bonded to the metal. More recently, the notion that they are disulfido complexes has been advocated.[2] The molecular S_2 or Se_2 description suggests that the formal oxidation state of the rhodium and iridium atoms be assigned as d^8 M(I).[34] Table VIII indicates that the actual metal d-electron configuration may be described approximately as d^8.

Table VII shows that $[Ir(S_2)(PH_3)_4]^+$ is related to the C_{2v} fragment $[Ir(PH_3)_4]^{3+}$ by a 1.64-e oxidation of the $Ir(PH_3)_4$ core (0.36 e is lost with the S_2 group). However, the increase in Ir atom charge that accompanies this oxidation is only 0.56 e, the remainder of the charge coming from the PH_3 ligands. This type of behavior, in which an n-e oxidation of a metal complex causes the charge of the metal atom to increase by much less than n, has been shown by ^{193}Ir Mössbauer spectroscopy to be characteristic of phosphine and carbonyl complexes of iridium. For these compounds, it is found in general that the electronic configuration of the metal is relatively insensitive to oxidation or reduction of the complex.[35,36]

Table VIII shows that the metal atom electronic configuration is very similar in $[M(S_2)(PH_3)_4]^+$ and $[M(Se_2)(PH_3)_4]^+$. For both Rh and Ir, in going from the S_2 to the Se_2 complex, there is a small increase in nd and $(n+1)$p orbital occupancy and essentially no change in $(n+1)$s orbital occupancy. In the case of iridium, the orbital occupancy differences may be used to roughly estimate the expected difference in ^{193}Ir Mössbauer isomer shifts of the S_2 and Se_2 complexes, for comparison with the measured difference for $[Ir(S_2)(dppe)_2]Cl$ and $[Ir(Se_2)(dppe)_2]Cl$.[6] The isomer shifts are directly proportional to $\Delta|\Psi(0)|^2$, the difference between the total s-electron densities at the nucleus in the source and absorber; they are a very sensitive probe of the Ir atom electronic environment. 6s electrons directly increase $|\Psi(0)|^2$ while 5d and $6p_{3/2}$ electrons decrease it by shielding the s electrons from the nucleus. A $6p_{1/2}$ electron makes a direct contribution to increasing $|\Psi(0)|^2$, but in the presence of a 6s electron its shielding effect on the 6s electron outweighs the direct contribution and it will reduce $|\Psi(0)|^2$. From the Dirac–Fock calculations of Mann (as cited by Wagner[37]), on $Au^{3+}(5d^8)$

(33) P. M. Treichel and G. P. Werber, *J. Am. Chem. Soc.* **90**, 1753 (1968).

(34) Assigning oxidation numbers in situations where the bonding is essentially covalent is a questionable exercise (for a discussion of this see F. A. Cotton and G. Wilkinson, "Advanced Inorganic Chemistry", 3rd ed., Interscience, New York, 1972, p 718). In the present case calling the metal d^8 M(I) suppresses the fact that there is charge in the $(n+1)$s and $(n+1)$p orbitals. In other instances the oxidation-state assignment is even more misleading; for example, in $[Ir(PH_3)_4]^{3+}$, the iridium is formally d^6 Ir(III) while the calculated 5d occupancy is approximately 8.

(35) A. F. Williams, G. C. H. Jones, and A. G. Maddock, *J. Chem. Soc.*, 1952 (1975).

(36) A. F. Williams, S. Bhaduri, and A. G. Maddock, *J. Chem. Soc.*, 1958 (1975).

(37) F. E. Wagner and U. Wagner in "Mössbauer Isomer Shifts", G. K. Shenoy and F. E. Wagner, Eds., North-Holland Publishing Co., Amsterdam, 1978, p 455.

Table X. Electronic Absorptions and Assignments for $[Rh(S_2)(dppe)_2]^+$

obsd values[a]			C_{2v} transition and excited state	calcd energy,[b] eV	predicted intens[c]	orbital description[d]
λ_{max}, nm	energy, eV	ϵ, M^{-1} cm^{-1}				
629	1.97	62	$4a_2 \rightarrow 7b_1(^1B_2)$	2.43	w	$\pi_\perp^* \rightarrow \pi_\parallel^*$, $p\sigma^*$, xz
541	2.29	1.9×10^2	$6b_1 \rightarrow 7b_1(^3A_1)$	3.06	w	$\pi_\parallel^* \rightarrow \pi_\parallel^*$, $p\sigma^*$, xz
345	3.59	1.0×10^4	$6b_1 \rightarrow 7b_1(^1A_1)$	3.46	s	$\pi_\parallel^* \rightarrow \pi_\parallel^*$, $p\sigma^*$, xz
306	4.05	2.6×10^4	$10a_1 \rightarrow 7b_1(^1B_1)$	3.82	s	$z^2, x^2-y^2 \rightarrow \pi_\parallel^*$, $p\sigma^*$, xz
			$6b_1 \rightarrow 11a_1(^1B_1)$	3.92	s	$\pi_\parallel^* \rightarrow x^2-y^2, z^2$
			$4a_2 \rightarrow 8b_1(^1B_2)$	3.98	s	$\pi_\perp^* \rightarrow p\sigma^*$, $s\sigma^*$

[a] Spectra of samples dissolved in EPA glasses at liquid-nitrogen temperature; measured from 300 to 800 nm. Extinction coefficients are corrected for solvent contraction on cooling to liquid-nitrogen temperature. [b] Spin-unrestricted transition-state calculations. [c] Dipole-allowed, spin-allowed transitions were classified as s (strong) or w (weak) on the basis of the orbital description shown in the last column: Transitions are called strong if they contain an $M \rightarrow L$ or $L \rightarrow M$ ($L = S_2$, Se_2) charge-transfer component between orbitals having most of their charge density in the same plane; they are also called strong if there is an intraligand (S_2, Se_2) component transition between orbitals with coincident charge density. If all of the components are $M \rightarrow L$ or $L \rightarrow M$ charge transfer, or intraligand transitions, between orbitals having most of their charge density in orthoganol planes, the transition is called weak. d–d transitions are taken to make a weak or medium contribution to the intensity. Dipole-allowed, spin-forbidden transitions are called weak if the corresponding spin-allowed transition is strong; otherwise they are called very weak (vw). Dipole-forbidden transitions are called very weak. All of the assigned transitions are dipole allowed. [d] The important components contributing to the transition.

Table XI. Electronic Absorptions and Assignments for $[Ir(S_2)(dppe)_2]^+$ [a]

obsd values			C_{2v} transition and excited state	calcd energy, eV	predicted intens	orbital description
λ_{max}, nm	energy, eV	ϵ, M^{-1} cm^{-1}				
582	2.13	13	$4a_2 \rightarrow 7b_1(^3B_2)$	2.25	vw	$\pi_\perp^* \rightarrow \pi_\parallel^*$, $p\sigma^*$, xz
530	2.34	1.3×10^2	$4a_2 \rightarrow 7b_1(^1B_2)$	2.85	w	$\pi_\perp^* \rightarrow \pi_\parallel^*$, $p\sigma^*$, xz
440	2.82	2.7×10^2	$4a_2 \rightarrow 8b_1(^3B_2)$	3.50	w	$\pi_\perp^* \rightarrow p\sigma^*$, $s\sigma^*$, $\pi_\parallel^*$
~340	~3.65 (poorly defined sh)		$6b_1 \rightarrow 7b_1(^3A_1)$	3.70	w	$\pi_\parallel^* \rightarrow \pi_\parallel^*$, $p\sigma^*$, xz
			$10a_1 \rightarrow 7b_1(^3B_1)$	3.74	w	$z^2, x^2-y^2 \rightarrow \pi_\perp^*$, $p\sigma^*$, xz
310	4.00	7.8×10^3	$4a_2 \rightarrow 8b_1(^1B_2)$	4.07	s	$\pi_\perp^* \rightarrow p\sigma^*$, $s\sigma^*$, $\pi_\parallel^*$
			$10a_1 \rightarrow 7b_1(^1B_1)$	4.09	s	$z^2, x^2-y^2 \rightarrow \pi_\parallel^*$, $p\sigma^*$, xz
			$6b_1 \rightarrow 7b_1(^1A_1)$	4.15	s	$\pi_\parallel^* \rightarrow \pi_\parallel^*$, $p\sigma^*$, xz

[a] See footnotes *a–d* of Table X and apply their respective citations to this table.

Table XII. Electronic Absorptions and Assignments for $[Rh(Se_2)(dmpe)_2]^+$ [a]

obsd values			C_{2v} transition and excited state	calcd energy, eV	predicted intens	orbital description
λ_{max}, nm	energy, eV	ϵ, M^{-1} cm^{-1}				
708	1.75	70	$4a_2 \rightarrow 7b_1(^1B_2)$	2.17	w	$\pi_\perp^* \rightarrow \pi_\parallel^*$, $p\sigma^*$, xz
617	2.01	48	$6b_1 \rightarrow 7b_1(^3A_1)$	2.87	w	$\pi_\parallel^* \rightarrow \pi_\parallel^*$, $p\sigma^*$, xz
			$4a_2 \rightarrow 8b_1(^3B_2)$	2.94	w	$\pi_\perp^* \rightarrow p\sigma^*$, $s\sigma^*$
459	2.70	1.0×10^2	$10a_1 \rightarrow 7b_1(^3B_1)$	3.30	w	$z^2, x^2-y^2 \rightarrow \pi_\parallel^*$, $p\sigma^*$, xz
389	3.19	7.2×10^2	$6b_1 \rightarrow 7b_1(^1A_1)$	3.24	s	$\pi_\parallel^* \rightarrow \pi_\parallel^*$, $p\sigma^*$, xz
310	4.00	1.2×10^4	$4a_2 \rightarrow 8b_1(^1B_2)$	3.55	s	$\pi_\perp^* \rightarrow p\sigma^*$, $s\sigma^*$
			$10a_1 \rightarrow 7b_1(^1B_1)$	3.67	s	$z^2, x^2-y^2 \rightarrow \pi_\parallel^*$, $p\sigma^*$, xz
			$6b_1 \rightarrow 11a_1(^1B_1)$	3.76	s	$\pi_\parallel^* \rightarrow x^2-y^2, z^2$

[a] See footnotes *a–d* of Table X and apply their respective citations to this table.

Table XIII. Electronic Absorptions and Assignments for $[Ir(Se_2)(dppe)_2]^+$ [a]

obsd values			C_{2v} transition and excited state	calcd energy, eV	predicted intens	orbital description
λ_{max}, nm	energy, eV	ϵ, M^{-1} cm^{-1}				
670	1.85	59	$4a_2 \rightarrow 7b_1(^3B_2)$	1.98	vw	$\pi_\perp^* \rightarrow p\sigma^*$, $\pi_\parallel^*$, xz
590	2.10	1.4×10^2	$4a_2 \rightarrow 7b_1(^1B_2)$	2.54	w	$\pi_\perp^* \rightarrow p\sigma^*$, $\pi_\parallel^*$, xz
462	2.68	2.3×10^2	$4a_2 \rightarrow 8b_1(^3B_2)$	3.30	w	$\pi_\perp^* \rightarrow p\sigma^*$, $\pi_\parallel^*$, $s\sigma^*$
452 (sh)	2.74 (sh)	2.0×10^2	$6b_1 \rightarrow 7b_1(^3A_1)$	3.42	w	$\pi_\parallel^* \rightarrow p\sigma^*$, $\pi_\parallel^*$, xz
390	3.18	3.1×10^2	$10a_1 \rightarrow 7b_1(^3B_1)$	3.61	w	$z^2, x^2-y^2 \rightarrow p\sigma^*$, $\pi_\parallel^*$, xz
330	3.76	5.1×10^3	$4a_2 \rightarrow 8b_1(^1B_2)$	3.76	s	$\pi_\perp^* \rightarrow p\sigma^*$, $\pi_\parallel^*$, $s\sigma^*$
			$6b_1 \rightarrow 7b_1(^1A_1)$	3.81	s	$\pi_\parallel^* \rightarrow p\sigma^*$, $\pi_\parallel^*$, xz
309	4.01	7.8×10^3	$10a_1 \rightarrow 7b_1(^1B_1)$	3.93	s	$z^2, x^2-y^2 \rightarrow p\sigma^*$, $\pi_\parallel^*$, xz

[a] See footnotes *a–d* of Table X and apply their respective citations to this table.

and $Au^{2+}(5d^86s)$, the contributions of the valence electrons to $|\Psi(0)|^2$ are +198 a_0^{-3} for a 6s electron, −25 a_0^{-3} for a 5d electron, −10 a_0^{-3} for a $6p_{1/2}$ electron, and −18 a_0^{-3} for a $6p_{3/2}$ electron. With these values, the results in Table VIII lead to $|\Psi(0)|^2(IrSe_2) - |\Psi(0)|^2(IrS_2) = -0.67\ a_0^{-3}$. From the relation[38] IS (mm s^{-1}) = $\beta(\Delta|\Psi(0)|^2)(\Delta\langle r^2\rangle)$, with $\beta = 6.4$ fm^{-2} a_0^3 mm s^{-1} and $\Delta\langle r^2\rangle = 5.5 \times 10^{-3}$ fm^2,[39] the change in $|\Psi(0)|^2$ corresponds to an isomer shift decrease of −0.024 mm s^{-1}. The experimental value is −0.059 mm s^{-1}.[6]

Comparison of the metal orbitals of the Rh and Ir complexes shows that the occupancy of Ir 6p is 0.2 e greater than that of Rh 5p and that the occupancy of Ir 6s is 0.25 e greater than

(38) G. K. Shenoy and B. D. Dunlap, ref 37, pp 890–894.

(39) F. E. Wagner and U. Wagner, ref 37, p 435.

that of Rh 5s. The change in the net atomic charge is smaller than the increase in sp-orbital occupancy since there is a parly compensating decrease in occupancy of the Ir 5d compared to the Rh 4d orbital. These changes in d- and p-orbital occupancy in going from a Rh to the corresponding Ir complex are mostly a manifestation of enhanced p_x- and p_z-orbital participation in Ir–X_2 bonding. The increased s-orbital occupancy for Ir compared to Rh must be associated only with Ir–P bonding since it is also found in the $[Ir(PH_3)_4]^{3+}$ fragment.

Relativistic Effects. Relativistic contributions are known to play an important role in the valence electronic structure of elements with atomic number greater than 69.[40] For this reason relativistic mass velocity and Darwin terms were included in the calculations for the iridium complexes. Since these corrections turn out to be chemically significant, we discuss their effects in this section.

In general, relativistic effects are expected to contract the orbital radii and lower the energy of s and p electrons and to expand the orbital radii and raise the energy of d electrons.[40] Figure 4 shows the effect of the relativistic corrections on the energy-level diagram of $[Ir(S_2)(PH_3)_4]^+$. At first sight the changes appear to be small, but a closer examination reveals that the relativistic effects have caused a significant increase in the Ir–S_2 interaction. This occurs in both levels $6b_1$ (in-plane π interaction) and $9a_1$ (σ interaction) where wave function contour maps show an increase in Ir–S_2 overlap.

In level $6b_1$ the improved π overlap results from the relativistic expansion of the d_{xz} orbital; the composition of the level is not significantly affected by the relativistic correction.[29] Because of enhanced π Ir–S_2 overlap, the $7b_1$–$6b_1$ splitting is 0.28 eV greater in the relativistic than in the nonrelativistic case. Enhanced π interaction of S_2 with Ir as compared to Rh is partly relativistic and partly nonrelativistic in origin. The nonrelativistic enhancement causes the $7b_1$–$6b_1$ splitting to increase from 3.23 eV in the RhS_2 complex to 3.64 eV in the nonrelativistic IrS_2 case.

In level $9a_1$ the relativistic effects lead to a 12% increase in $6p_z$-orbital participation[30] at the expense of $5d_{z^2}$ and $5d_{x^2-y^2}$. This, combined with d-orbital expansion, gives the hybrid greater extension in the z direction and leads to improved σ Ir–S_2 overlap. The energy of level $9a_1$ is essentially the same in both the relativistic and nonrelativistic cases, presumably because the relativistic increase in d-orbital energy cancels the decrease in energy due to improved overlap. Since nonrelativistic σ Ir–S_2 overlap in level $9a_1$ is essentially the same as σ Rh–S_2 overlap, the increase in σ M–S_2 interaction in going from Rh to Ir must be almost entirely a relativistic effect.

The net increase in Ir–S_2 interaction caused by relativistic effects is clearly seen by comparing the total valence charge density maps for the relativistic (Figure 8c) and nonrelativistic (Figure 9) cases. The nonrelativistic enhancement of net Ir–S_2 with respect to net Rh–S_2 interaction is evident from a comparison of Figures 8a and 9. A significant part of the overall increase in the net M–S_2 interaction in going from Rh to Ir is clearly a relativistic effect.

Another relativistic effect that should be mentioned is an increase of 0.2 e in Ir 6s-orbital occupancy. This accounts for most of the 0.25-e increase in s-orbital occupancy that we noted in comparing Rh and Ir complexes. Since increased 6s-orbital occupancy in the iridium complexes does not have a significant effect on Ir–X_2 bonding, we will not analyze it in detail.

M–P Bonding. Table IX summarizes the orbitals in which M–P interaction occurs. There are no unusual features in the M–P bonding, and we will not discuss it in detail. The most important metal orbitals for bonding the equatorial phosphorus atoms are nd_{xz} and $(n + 1)$s; the axial phosphorus atoms are primarily bound through $nd_{x^2-y^2}$ and nd_{yz}. M(d)→P(3d) back-bonding occurs in orbital $10a_1$ in all four complexes. The phosphorus atom contribution to level $10a_1$ has from 22 to 45% 3d character (Table IX), compared to 0% 3d character for the PH_3 lone-pair orbital before complexation. Since orbital $10a_1$ has much more metal than P character, its P 3d character may be taken to represent M(d)→P(3d) back-bonding.

Optical Spectrum. Assignments (Tables X–XIII) were made by associating the observed bands with the transitions they most nearly match in energy and predicted intensity. However, the lowest energy bands in $[Rh(S_2)(Ph_3)_4]^+$ and $[Rh(Se_2)(PH_3)_4]^+$ were assigned as $4a_2 \rightarrow 7b_1(^1B_2)$ even though assignment as $4a_2 \rightarrow 7b_1(^3B_2)$ gives better agreement with the calculated transition energy. This was done to avoid the anomaly of having the triplet transition more intense in the Rh than in the corresponding Ir complex. Also, in the case of $[Rh(Se_2)(PH_3)_4]^+$, assignment of the 708-nm band as $4a_2 \rightarrow 7b_1(^3B_2)$ leads to the assignment of the 617-nm band as the corresponding singlet transition, which is inconsistent with its intensity. It appears that only in the case of the Ir complexes, with their larger spin–orbit coupling, is the $4a_2 \rightarrow 7b_1(^3B_2)$ transition observed. We regard the assignments as satisfactory in the sense that (1) all orbitally allowed singlet transitions expected in the ~300–800-nm range are accounted for, (2) in the Ir complexes, the triplet transitions corresponding to all of the observed singlet transitions are also accounted for, and (3) the calculated transition energies are mostly in reasonable agreement with the observed band energies.

Comparison of the spectra of $[Rh(S_2)(dppe)_2]^+$ (Table X) and $[Ir(S_2)(dppe)_2]^+$ (Table XI) shows that the bands in the Ir complex are shifted to higher energy; this shift is due to the enhanced M–S_2 interaction in the iridium complex. The energy of transition $6b_1 \rightarrow 7b_1$ is a measure of the strength of the π component of the M–S_2 interaction. The shift in the calculated value of this transition energy from the Rh to the Ir complex to +0.64 eV for the triplet and +0.69 eV for the singlet; the observed shift of the band assigned as $6b_1 \rightarrow 7b_1(^1A_1)$ is +0.56 eV. Increasing the basicity of the phosphine ligand by changing from dppe to dmpe causes a blue shift in the $6b_1 \rightarrow 7b_1$ transition; we estimate the shift in $6b_1 \rightarrow 7b_1(^1A_1)$ to be +0.9 eV in the IrS_2 complexes and +0.25 eV in the RhS_2 complexes.[41] Figure 5 provides an explanation for these observations. There is evidently a P–X_2 bonding interaction that contributes to the π M–X_2 interaction. Increasing the basicity of the phosphine enhances the P–X_2 overlap and increases the π M–X_2 bonding and $6b_1$–$7b_1$ splitting. The effect is greater for the iridium complexes becasue they have a larger P–X_2 interaction (cf. parts a and c of Figure 5).

Reactivity of Rhodium and Iridium Disulfur and Diselenium Complexes. The known reactions of side-on-bonded S_2 and Se_2 complexes of rhodium and iridium[6] may be rationalized in terms of addition of electrons to the LUMO and removal or coordination of electrons from the HOMO. Electrochemical reduction of $[Ir(X_2)(dppe)_2]^+$ ($X_2 = O_2$, S_2, Se_2), which takes place according to the equation

$$[Ir(X_2)(dppe)_2]^+ + e^- \rightarrow [Ir(dppe)_2]^+ + X_2^-$$

is the simplest example of electron addition to the LUMO.[42] This reaction confirms that the LUMO is MX_2 antibonding.

An important reaction of $[M(X_2)(L\text{–}L)_2]^+$ (M = Rh, Ir; $X_2 = S_2$, Se_2; L–L = dppe, dmpe) is the addition of low-valent group 8 metal complexes across the S–S or Se–Se bond to form

(40) For reviews see: K. S. Pitzer, *Acc. Chem. Res.*, **12**, 271 (1979); P. Pyykö and J. P. Desclaux, *ibid.* **12**, 276 (1979).

(41) A. P. Ginsberg and C. R. Sprinkle, unpublished results.

(42) B. K. Teo, A. P. Ginsberg, and J. C. Calabrese, *J. Am. Chem. Soc.*, **98**, 3027 (1976).

heterometallic $(\mu\text{-}S)_2$ dimers, for example

$$[Ir(S_2)(dppe)_2]^+ + PtL_3 \rightarrow [(dppe)_2Ir(\mu\text{-}S)_2PtL_2]^+ + L$$

(L = PPh_3, $PEtPh_2$). In this reaction, PtL_3 presumably first dissociates to PtL_2,[43] which then reacts with the S_2 complex. A simple way to interpret the addition reaction is to assume that it begins with corrdination of PtL_2 via donation from Pt $5d_{xz}$ into the LUMO. The $\pi_\parallel^*$ and $p\sigma^*$ character of the LUMO favors rupture of the S–S bond and formation of the $(\mu\text{-}S)_2$ complex:

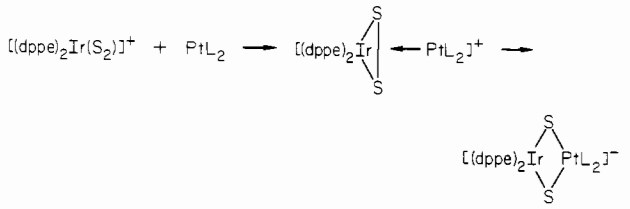

As expected for this mechanism, increasing the basicity of ligand L facilitates insertion of Pt into the S–S bond.

I_2 adds to $[Ir(S_2)(dppe)_2]Cl$ with rupture of the I–I bond and formation of the cis-octahedral complex $[Ir(SI)_2(dppe)_2]Cl$. The I_2 molecule has a ground-state valence-electron configuration of $...(5p\sigma)^2(5p\pi)^4(5p\pi^*)^4$, with an ionization potential of 9.28 eV and a transition to the first excited electronic configuration, $...(5p\sigma^2)(5p\pi)^4(5p\pi^*)^3(5p\sigma^*)^1$, near 520 nm. The I_2 HOMO, $5p\pi^*$, and LUMO, $5p\sigma^*$, are therefore respectively at ~–9.3 and ~–6.9 eV. In its reaction with $[Ir(X_2(L\text{–}L)_2]^+$ (X = S, Se), I_2 is therefore expected to be a very poor donor but a good acceptor for the electrons in levels $4a_2$ and $6b_1$. For maximum overlap of orbital $4a_2$ or $6b_1$ with the I_2 σ^* MO, an end-on approach of the I_2 molecule to the X_2 group, as depicted in (1) for interaction with the $4a_2$

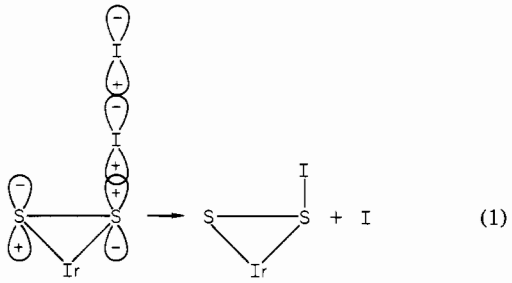

(1)

orbital, is required; we assume this to be the first step in addition of I_2 to $[Ir(S_2)(dppe)_2]^+$ and that it leads to rupture of the I–I bond. A subsequent interaction of the same type between an I_2 molecule and the $6b_1$ orbital would lead to the observed product. The related complex $[Ir(SO)_2(dppe)_2]^+$, which has the structure[44] I, has been shown to be formed in

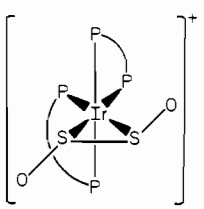

I

a two-step oxidation of $[Ir(S_2)(dppe)_2]^+$ by periodate.[45] Interaction of two IO_4^- ions with the $4a_2$ and $6b_1$ orbitals, similar to what we have suggested above for the I_2 addition reaction, would account for the formation of $[Ir(SO)_2(dppe)_2]^+$. An important difference between $[Ir(SO)_2(dppe)_2]^+$ and $[Ir(SI)_2(dppe)_2]^+$ is the presence of two additional valence electrons in the latter compound; these presumably occupy orbital $7b_1$, the LUMO of the S_2 complex. We therefore expect that in the SI complex the Ir–S and S–S bonds are weakened in comparison to the SO complex.

The observations that have been made[6] on the effect of the metal (Rh, Ir) and the ligand (dppe, dmpe) on the reactivity of $[M(X_2)(L\text{–}L)_2]^+$ (X = S, Se) are consistent with the results of our calculations. For example, the observations that, for corresponding complexes, mercury strips sulfur or selenium much more readily from rhodium than from iridium and that it strips Se much more readily than S may be understood in terms of the ordering we have found for the relative strength of the $M\text{–}X_2$ covalent interaction. Increasing the basicity of ligand L–L (i.e., changing from dppe to dmpe) causes a large decrease in the rate at which Hg strips sulfur or selenium from the complexes. This effect is attributed to the $P\text{–}S_2$ bonding interaction in level $6b_1$, which we have already discussed as the cause of the spectral blue shift in the $6b_1 \rightarrow 7b_1(^1A_1)$ transition of $[M(S_2)(L\text{–}L)_2]^+$.

Comparison of M–O_2, M–S_2, and M–Se_2 Bonding. We have seen that in the complexes $[M(X_2)(PH_3)_4]^+$ (M = Rh, Ir) the bondings of S_2 and of Se_2 are very similar; the only important difference is that the covalent interaction is significantly weaker for $M\text{–}Se_2$ than for $M\text{–}S_2$. Our results for $M\text{–}S_2$ and $M\text{–}Se_2$ bonding may be compared with Norman's SCF–Xα-based description of $M\text{–}O_2$ bonding in $[Pt(O_2)(PH_3)_2]$[11] and $[M(O_2)(PH_3)_4]^+$ (M = Rh, Ir).[10] The major differences are as follows: (1) In-plane covalent π interaction is much greater for $M\text{–}S_2$ and $M\text{–}Se_2$ than for $M\text{–}O_2$. (2) σ $M\text{–}X_2$ overlap is greater for $M\text{–}O_2$ than for $M\text{–}S_2$ or $M\text{–}Se_2$. (3) Comparison of total valence charge density maps indicates that the net covalent $Pt\text{–}O_2$ interaction is similar to the $Ir\text{–}Se_2$ and less than the $Ir\text{–}S_2$ interaction. (4) $[M(O_2)(PH_3)_4]^+$ was described in terms of formal oxidation states as a d^6 M(III) complex of O_2^{2-}.[10] The contrast with our description of the disulfur and diselenium analogues as complexes of *molecular* S_2 or Se_2 is misleading in that it implies a drastic difference in electronic structure that does not in fact exist. In particular, the calculated metal 5d occupancy for $[M(O_2)(PH_3)_4]^+$ is approximately 8,[46] as it is in the disulfur and diselenium complexes, and the net charge on O_2 is ca. 0.4–,[46] similar to what is found for S_2 and Se_2. It is also clear from the small difference betwen $[Ir(O_2)(dppe)_2]^+$ and $[Ir(S_2)(dppe)_2]^+$ ^{193}Ir Mössbauer isomer shifts[6] $(IS(IrS_2) - IS(IrO_2) = -0.084$ mm $s^{-1})$ that the Ir atom electronic environments are very similar in the O_2 and S_2 complexes. Our statement that the complexed S_2 and Se_2 groups should be thought of as molecules in an excited state with configuration $...(p\sigma)^2(\pi)^3(\pi^*)$ is an approximate description of the Xα results that is equally applicable to the Xα results for $[M(O_2)(PH_3)_4]^+$ and $Pt(O_2)(PH_3)_2$.[11b] By adopting this description for the O_2, as well as the S_2 and Se_2 complexes, we arrive at a bonding model that emphasizes the similarities between these compounds and does not suggest nonexistent differences. The d^6 M(III)–O_2^{2-} description of $[M(O_2)(PH_3)_4]^+$ is based on an interpretation of the frontier orbitals, according to which levels $10a_1$, $5b_2$, and $3a_2$, which fall immediately below the nominal O_2 $\pi_\perp^*$ and $\pi_\parallel^*$ levels, are identified with the three t_{2g} orbitals (d_{xy}, d_{yz}, and d_{z^2}) expected for six-coordinate d^6 M(III), while the two unoccupied levels ($7b_1$ and $11a_1$) are identified with the e_g orbitals (d_{xz} and $d_{x^2-y^2}$). A similar interpretation of the frontier orbitals for the S_2 and Se_2 complexes is not plausible.

A final point that should be noted in comparing the Xα results for the rhodium and iridium O_2, S_2, and Se_2 complexes is that the order of the two lowest unoccupied orbitals is $11a_1$

(43) F. R. Hartley, "The Chemistry of Platinum and Palladium", Wiley, New York, 1973, p 33.
(44) G. Schmid and G. Ritter, *Chem. Ber.*, **108**, 3008 (1975).
(45) G. Schmid and G. Ritter, *Angew. Chem., Int. Ed. Engl.*, **14**, 645 (1975).
(46) J. G. Norman, Jr., personal communication.

$< 7b_1$ for the O_2 and complexes, but it is $7b_1 < 11a_1$ for the S_2 and Se_2 complexes. Orbital $11a_1$ is primarily $M-P_{ax}$ antibonding in character while $7b_1$ is strongly X-X and $M-X_2$ antibonding. The ordering of the levels in the two cases is different because of the different $P_{ax}-Ir-P_{ax}$ angles used in the calculations. For both the Rh and Ir dioxygen complexes the $P_{ax}-Ir-P_{ax}$ angle was taken to be 161°, the same as the angle in $[M(O_2)(P(CH_3)_2C_6H_5)_4]^+$ (M = Rh, Ir), but for the S_2 and Se_2 complexes the angle used was 172°, the same as the angle in $[Ir(X_2)(dppe)]^+$ (X = S, Se) and close to the angle (175°) in $[Ir(O_2)(dppe)_2]^+$. The more nearly linear angle in the S_2 and Se_2 complexes increases the $M-P_{ax}$ antibonding interaction in orbital $11a_1$ and raises it above $7b_1$. Since the behavior of $[Ir(O)_2(dppe)_2]^+$ on electrochemical reduction indicates that it has a strongly $Ir-O_2$ antibonding LUMO,[42] it is likely that the LUMO of this complex is orbital $7b_1$, as would be anticipated from its nearly linear $P_{ax}-M-P_{ax}$ angle.

Acknowledgment. We are indebted to Professor J. G. Norman, Jr., for informing us of the details of his calculations on dioxygen complexes prior to publication.

Registry No. $[Rh(S_2)(PH_3)_4]^+$, 83632-71-7; $[Rh(Se_2)(PH_3)_4]^+$, 83632-72-8; $[Ir(S_2)(PH_3)_4]^+$, 83632-73-9; $[Ir(S_2)(PH_3)_4]^+$, 83632-74-0; $[Ir(PH_3)_4]^{3+}$, 82269-54-3; S_2^{2-}, 16734-12-6.

Contribution from the Department of Chemistry,
The University of Arizona, Tucson, Arizona 85721

1,4,7-Trithiacyclononane, a Novel Tridentate Thioether Ligand, and the Structures of Its Nickel(II), Cobalt(II), and Copper(II) Complexes

WILLIAM N. SETZER, CRAIG A. OGLE, GEORGE S. WILSON, and RICHARD S. GLASS*

Received December 3, 1981

An improved method for preparing 1,4,7-trithiacyclononane (1,4,7-TTCN) is reported. The yields of certain medium-sized-ring dithioethers are also improved by this method. The bis(1,4,7-trithiacyclononane)nickel(II), -cobalt(II), and -copper(II) complexes have been prepared and their structures determined by X-ray crystallographic analyses. The $[Ni(1,4,7\text{-}TTCN)_2](BF_4)_2$ complex crystallizes in the monoclinic space group $P2_1/c$ with $a = 8.681$ (2) Å, $b = 11.685$ (3) Å, $c = 11.624$ (3) Å, $\beta = 106.57$ (2)°, and $Z = 2$. The $[Co(1,4,7\text{-}TTCN)_2](BF_4)_2$ complex crystallizes in the orthorhombic space group *Pbca* with $a = 19.789$ (40) Å, $b = 15.235$ (12) Å, $c = 9.202$ (3) Å, and $Z = 4$. The $[Cu(1,4,7\text{-}TTCN)_2](BF_4)_2$ complex crystallizes in the orthorhombic space group *Pbca* with $a = 21.169$ (3) Å, $b = 15.193$ (2) Å, $c = 8.729$ (2) Å, and $Z = 4$. Full-matrix least-squares refinement led to convergence with $R = 0.030$, 0.094, and 0.062, respectively, after several cycles of anisotropic refinement. In each complex the metal atom occupies a slightly distorted octahedral environment of sulfur atoms provided by two facially coordinating 1,4,7-TTCN ligands. The geometrical constraints of the ligand induce nearly regular octahedral coordination even with copper(II).

Introduction

Transition-metal complexes with thioether ligands are of much current interest. Such complexes have been extensively reviewed recently.[1] Of particular interest from a biological perspective are the copper complexes of thioethers. Macrocyclic tetrathioether complexes of Cu(II), even those with undistorted tetragonal coordination geometry about the copper atom,[2] show the same unusual spectroscopic[3] and electrochemical properties[4] as the "blue" copper proteins. Coordination of all four sulfur atoms of a macrocyclic tetrathioether such as 1,4,8,11-tetrathiacyclotetradecane (14-ane-S_4) by a single metal atom requires a change in conformation of the ligand. Crystal structure studies show that the conformation of the uncomplexed 14-ane-S_4[5] is one in which the sulfur atoms are all directed away from the center of the ring, i.e., exodentate. However, in its Cu(II)[2] and Ni(II)[6] complexes, in which all four sulfur atoms are coordinated to the metal atom in a planar array, the ligand adopts an endodentate conformation. Our structural studies of crystalline[7] and gaseous[8] 1,4,7-trithiacyclononane (1,4,7-TTCN) revealed that, unlike macrocyclic polythioethers,[5,9] it adopts a conformation with the sulfur atoms endodentate. In this conformation 1,4,7-TTCN can be a tridentate ligand without conformational change[10] and owing to the geometric placement of the three ligating sulfur atoms suitable metal complexes may be unusually stable.[11]

This paper reports an improved procedure for preparing 1,4,7-TTCN and the crystal and molecular structure of $[Ni(1,4,7\text{-}TTCN)_2](BF_4)_2$, $[Co(1,4,7\text{-}TTCN)_2](BF_4)_2$, and $[Cu(1,4,7\text{-}TTCN)_2](BF_4)_2$.

Experimental Section

Preparation of 1,4,7-Trithiacyclononane—Typical Procedure for Preparation of Mesocyclic Polythioethers. A 2-L three-necked round-bottom flask, equipped with matching calibrated 125-mL

(1) Murray, S. G.; Hartley, F. R. *Chem. Rev.* **1981**, *81*, 365.
(2) Glick, M. D.; Gavel, D. P.; Diaddario, L. L.; Rorabacher, D. B. *Inorg. Chem.* **1976**, *15*, 1190. For recent model studies for blue copper proteins see: Ferris, N. S.; Woodruff, W. H.; Rorabacher, D. B.; Jones, T. E.; Ochrymowycz, L. A. *J. Am. Chem. Soc.* **1978**, *100*, 5939. Jones, M. H.; Levason, W.; McAuliffe, A. A.; Murray, S. G. *Bioinorg. Chem.* **1978**, *8*, 267. Dagdigian, J. V.; Reed, C. A. *Inorg. Chem.* **1979**, *18*, 2623. Sakaguchi, U.; Addison, A. W. *J. Chem. Soc., Dalton Trans.* **1979**, 600. Nikles, D. E.; Powers, M. J.; Urbach, F. L. *Inorg. Chim. Acta* **1979**, *37*, L499.
(3) Jones, T. E.; Rorabacher, D. B.; Ochrymowycz, L. A. *J. Am. Chem. Soc.* **1975**, *97*, 7485.
(4) Dockal, E. R.; Jones, T. E.; Sokol, W. F.; Engerer, R. J.; Rorabacher, D. B.; Ochrymowycz, L. A. *J. Am. Chem. Soc.* **1976**, *98*, 4322.
(5) DeSimone, R. E.; Glick, M. D. *J. Am. Chem. Soc.* **1976**, *98*, 762.
(6) Davis, P. H.; White, L. K.; Belford, R. L. *Inorg. Chem.* **1975**, *14*, 1753.
(7) Glass, R. S.; Wilson, G. S.; Setzer, W. N. *J. Am. Chem. Soc.* **1980**, *102*, 5068.
(8) Setzer, W. N.; Coleman, B. R.; Wilson, G. S.; Glass, R. S. *Tetrahedron* **1981**, *37*, 2743.
(9) Dalley, N. K.; Smith, J. S.; Larson, S. B.; Matheson, K. L.; Christensen, J. J.; Izatt, R. M. *J. Chem. Soc., Chem. Commun.* **1975**, 84.
(10) Coordination of exodentate macrocyclic polythioethers by first-row transition metal ions has been suggested to occur by initial metal attack on a sulfur atom of the more accessible exodentate conformer. Rearrangement then probably must occur to the endodentate conformation before a second sulfur atom coordinates: DeSimone, R. E.; Glick, M. D. *J. Coord. Chem.* **1976**, *5*, 181. Jones, T. E.; Zimmer, L. L.; Diaddario, L. L; Rorabacher, D. B.; Ochrymowycz, L. A. *J. Am. Chem. Soc.* **1975**, *97*, 7163. Diaddario, L. L.; Zimmer, L. L.; Jones, T. E.; Sokol, L. S. W. L.; Cruz, R. B.; Yee, E. L.; Ochrymowycz, L. A.; Rorabacher, D. B. *Ibid.* **1979**, *101*, 3511.
(11) Busch, D. H.; Farmery, K.; Goedken, V.; Katovic, V.; Melnyk, A. C.; Sperati, C. R.; Tokel, N. *Adv. Chem. Ser.* **1971**, *No. 100*, 52; Busch, D. H. *Acc. Chem. Res.* **1978**, *11*, 392.

0020-1669/83/1322-0266$01.50/0